Journal of
Marine Science and Engineering

MDPI

Article

The Impact of Sluice Construction in the North Branch of the Changjiang Estuary on Saltwater Intrusion and Freshwater Resources

Yidi Yang [1], Jianrong Zhu [1,*], Zhengbing Chen [2] and Rui Ma [1]

[1] State Key Laboratory of Estuarine and Coastal Research, East China Normal University, Shanghai 200241, China; y1085154266@163.com (Y.Y.); 52213904014@stu.ecnu.edu.cn (R.M.)
[2] Key Laboratory of Changjiang Regulation and Protection, Ministry of Water Resources, Changjiang Design Group Co., Ltd., Wuhan 430010, China; chenzhengbing@cjwsjy.com.cn
* Correspondence: jrzhu@sklec.ecnu.edu.cn

Abstract: Estuarine projects can quickly change the estuarine topography and influence the hydrodynamics and saltwater intrusion. The Changjiang Estuary is a multiple-bifurcation megaestuary, and the outstanding feature of the saltwater intrusion is the saltwater spillover from the North Branch (NB) into the South Branch (SB). In this study, the improved ECOM-si model was adopted to numerically experiment with the impact of the sluices that are planned for construction in the upper, middle, and lower reaches of the NB on the saltwater intrusion and freshwater resources. The simulation results show that, on the one hand, sluice construction can eliminate the saltwater spillover from the NB into the SB; on the other hand, sluice construction makes water enter the NB from the SB, and the runoff discharging into the sea in the SB decreases. The water intake time of the Qingcaosha Reservoir (QCSR) increases by 3.2 days for sluice construction in the upper reaches of the NB and decreases by 0.97 and 0.94 days for sluice construction in the middle and lower reaches of the NB, respectively. Considering the impact of sluice construction in the NB on the saltwater intrusion and freshwater resources, the construction of sluices in the upper reaches of the NB is recommended.

Keywords: numerical simulation; water transport; salt transport; salinity variation; estuarine projects; North Branch

check for updates

Citation: Yang, Y.; Zhu, J.; Chen, Z.; Ma, R. The Impact of Sluice Construction in the North Branch of the Changjiang Estuary on Saltwater Intrusion and Freshwater Resources. *J. Mar. Sci. Eng.* **2023**, *11*, 2107. https://doi.org/10.3390/jmse11112107

Academic Editor: Assimina Antonarakou

Received: 7 October 2023
Revised: 30 October 2023
Accepted: 1 November 2023
Published: 3 November 2023

1. Introduction

An estuary is an area where a river and the ocean merge. Freshwater from rivers and saltwater from the sea mix strongly in this area. Simultaneously, under the combined action of multiple factors, such as tides, meteorology, and continental-shelf circulation, saltwater moves upstream, forming a saltwater intrusion. Saltwater intrusion in estuaries is the main factor threatening the utilization of freshwater resources in delta regions, which is mainly controlled by runoff and tides, as well as by wind, topography, and sea level rise. Tides and runoff are the key factors affecting the saltwater intrusion in estuaries. Bowden et al. [1] found that there is a high correlation between the salinity and river discharge in the Mersey Estuary. Sassi et al. [2] pointed out that tides affect the division of river discharge and change the distributive ratios of river channels. Simpson et al. [3] pointed out that the freshwater buoyancy input can induce the stratification of coastal waters by driving the density current flow, which is regulated by tidal variations in vertical mixing. Gong et al. [4] indicated that the response of saltwater intrusion to change in the tidal velocity is largely dependent on the river discharge. Wind also has a great influence on saltwater intrusion. Different wind speeds, directions, and durations result in different strengths of the flood and ebb tidal currents in estuaries, and the influences on the saltwater intrusion in estuaries are also different [5]. Valle-Levinson et al. [6], via observations, indicated strong salinity variation during hurricanes. Li et al. [7] found a strong saltwater intrusion in Chesapeake

Bay due to the strong landward winds. Li et al. [8] found the disturbance of the salinity in the Pontchartrain Estuary from hurricanes Gustav and Ike. Gong et al. [9] indicated that the saltwater intrusion in the Pearl River Estuary was intensified by adding wind conditions to the model. Sea level rise is also a contributing factor, leading to more saltwater intrusion into estuaries [10,11]. Gong et al. [12] found that, after the sea level rise, the average salinity of Chesapeake Bay and the salt intrusion depth had an increasing trend. Bhuiyan et al. [13] found that, after a sea level rise of 59 cm, the salinity at 80 km upstream of the Gorai Estuary increased by 0.9. The influence of human activities on saltwater intrusion has also received extensive attention [14]. The impact of basin and estuary projects has a significant influence on saltwater intrusion. Basin projects, such as the Three Gorges Dam and the South-to-North Water Diversion Project, can seasonally regulate the river discharge and thereby affect the saltwater intrusion in estuaries [15–18]. The construction of estuarine projects artificially changes the local topography, resulting in a certain impact on the hydrodynamics and saltwater intrusion in estuaries [19–23].

The Changjiang Estuary is one of the most well-known estuaries in the world and is classified as a medium-strength tidal, multiple-bifurcation estuary. Chongming Island divides the Changjiang River into the North Branch (NB) and the South Branch (SB) to form the first bifurcation. Changxing Island and Hengsha Island divide the SB into the North Channel (NC) and the South Channel (SC) to form the second bifurcation. Finally, the Jiuduan Sandbank divides the SC into the North Passage and the South Passage to form the third bifurcation (Figure 1a). In addition to saltwater intrusion from the outer sea, there is also lateral saltwater intrusion due to water and salt exchange between different channels, making the changes in the saltwater intrusion in the Changjiang Estuary more complicated [24–26]. In the 17th century, the water diversion ratio (WDR) of the NB could reach 50%. By the beginning of the 20th century, the main channel of the Changjiang River had begun to shift to the SB, and the WDR of the NB dropped to 25%. Afterward, the volume of the NB continued to decrease and gradually tended to shrink. By the end of the 20th century, the upper reaches of the NB had severely narrowed and were nearly orthogonal to the SB. The lower reaches of the NB had become funnel-shaped, which increased the tidal range, which causes saltwater spillover from the NB to the SB, especially during the dry season [24,27]. The saltwater spillover from the NB seriously affects the freshwater resource utilization in the SB, which is a threat to freshwater resource utilization in the Changjiang Estuary.

Constructing reservoirs in estuaries is challenging due to saltwater intrusion [28–30]. When the salinity exceeds the drinking water standard (0.45 psu), it is unsuitable to use water from the river. There are several reservoirs in the SB, including the Taicang Reservoir, Dongfeng Xisha Reservoir, Chenhang Reservoir, and the world's largest estuarine reservoir, the Qingcaosha Reservoir (QCSR), which was built in 2010. The Taicang Reservoir in Suzhou city, Jiangsu Province, has an effective capacity of 15.0×10^6 m^3 and provides a daily water supply of 6.0×10^5 m^3. The Chenhang Reservoir has an effective capacity of 8.60×10^6 m^3 and provides a daily water supply of 2.06×10^6 m^3 for the 2 million people in Shanghai. The Dongfeng Xisha Reservoir has an effective capacity of 8.90×10^6 m^3 and provides a daily water supply of 2.1×10^5 m^3 for more than 700,000 people on Chongming Island, Shanghai. The QCSR has an effective capacity of 4.35×10^8 m^3 and provides a daily water supply of 7.19×10^6 m^3 for more than 13 million people in the main districts of Shanghai [31]. However, these reservoirs are often affected by saltwater intrusion [32]. In recent decades, the Changjiang Estuary has experienced multiple severe incidents of saltwater intrusion, such as the saltwater intrusion event in February 2014 under persistent strong northerly winds [5] and the severe saltwater intrusion event in late summer and autumn of 2022. These events posed very serious threats to the freshwater intake in the SB, and it is necessary to propose measures to mitigate the saltwater intrusion to ensure the safety of the freshwater resources of the reservoirs.

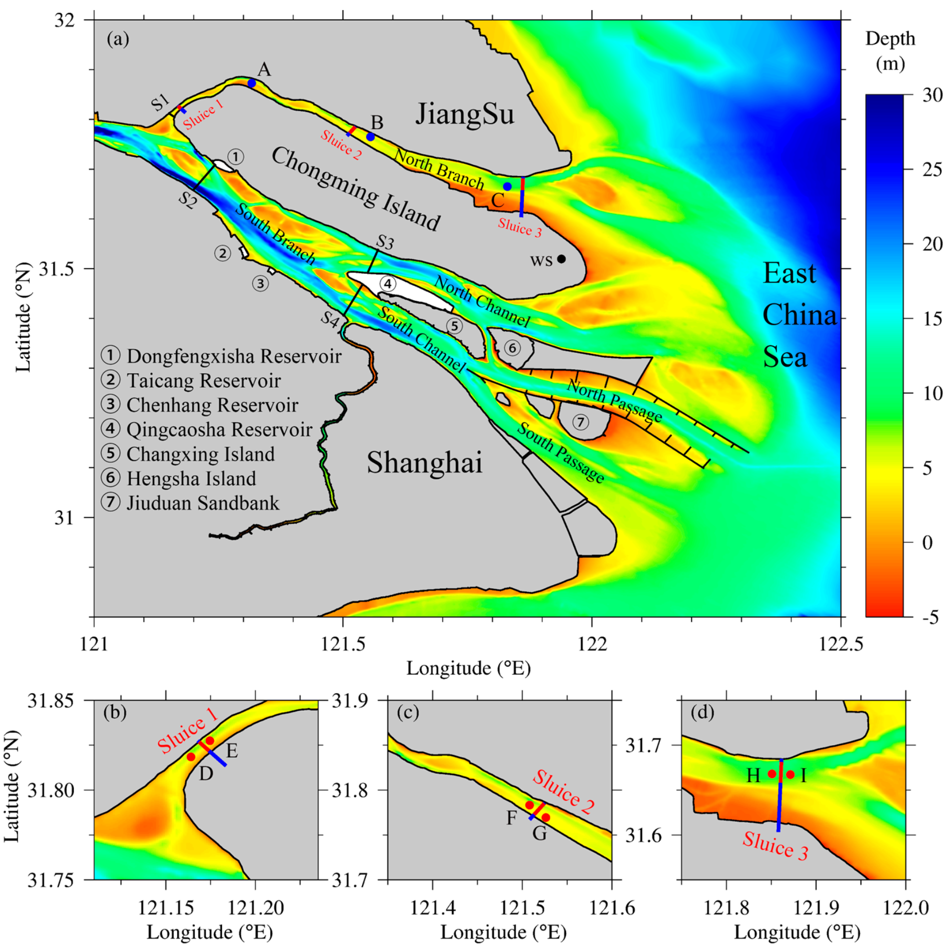

Figure 1. Topography of the Changjiang Estuary (**a**). White areas indicate the locations of the reservoirs. Sections are denoted by black lines. Red lines indicate sluices, and blue lines indicate embankments (the same hereinafter). Blue dots indicate the locations of three ship-measured sites: A, B, and C. Red dots (D–I) indicate sites upstream and downstream of sluices 1, 2, and 3 that are located in the upper (**b**), middle (**c**), and lower (**d**) reaches of the NB, respectively. WS is the location of the weather station at the Chongming Eastern Shoal.

One means of ensuring the safety of estuarine freshwater resources is to construct sluices to block saltwater intrusion. There are many well-known estuarine sluices worldwide, such as the Saemangeum Lake sluice in South Korea, which improves the water quality of Saemangeum Lake by regulating the operation of the sluice to control runoff into the sea [33]. The sluice in the Cao River Estuary of Zhejiang Province has resulted in comprehensive benefits, such as flood control, water resource utilization, and navigation [34]. After sluice construction in the Sheyang Estuary in Jiangsu Province, the reservoir capacity reached 3.08×10^7 m^3, which greatly improved the utilization of the water resources [35].

The saltwater intrusion in the NB is more severe compared to that in the SB, NC, SC, North Passage, and South Passage due to its funnel shape and low river discharge. Saltwater spillover from the NB into the SB is the most characteristic of saltwater intrusion in the Changjiang Estuary. All reservoirs in the Changjiang Estuary are built in the SB. The sources of the saltwater of the Chenhang, Dongfeng Xisha, and Taicang reservoirs are mainly from the saltwater spillover from the NB and rarely from saltwater intrusion from the NC and SC. The salinity at the water intake of the QCSR comes from both saltwater spillover from the NB and saltwater intrusion from the NC. The purpose of building a sluice in the NB is to weaken the saltwater intrusion from the NB and improve the water intake capacity of the reservoirs in the SB, but the effect of building a sluice is not clear, and where the sluice will be built in the NB for a better effect is also unknown. Therefore, this paper used a numerical model to simulate the effect of building a sluice in the NB on the saltwater intrusion and freshwater resources in the SB.

The remainder of this paper is organized as follows: Section 2 introduces the numerical models used herein, analytical methods, and setting of the numerical experiments. In Section 3, the results of the numerical simulation and some comparative analyses are given, including the salinity and current field before and after sluice construction. In Section 4, the differences in the salinity among the sluice constructions at different reaches of the NB are discussed. Finally, the conclusion is provided in Section 5.

2. Methods

2.1. Numerical-Model Configuration

The numerical model employed in this study is based on the ECOM-si (Estuarine, Coastal, and Ocean Model—semi-implicit), which is an extension of the POM (Princeton Ocean Model) [36]. The ECOM-si was developed under the hydrostatic assumption and the Boussinesq approximation. A non-orthogonal curvilinear coordinate transformation ($\xi = \xi(x,y)$, $\eta = \eta(x,y)$) was introduced into the horizontal direction, and a σ coordinate transformation ($\sigma = \frac{z-\zeta}{H+\zeta}$, σ varies from -1 at $z = -H$ to 0 at $z = \zeta$) was introduced into the vertical direction.

The momentum equations in the non-orthogonal curvilinear coordinates are given as follows [37]:

$$\begin{aligned}\frac{\partial DJu_1}{\partial t} + \frac{\partial DJ\hat{U}u_1}{\partial \xi} + \frac{\partial DJ\hat{V}u_1}{\partial \eta} + \frac{\partial J\omega u_1}{\partial \sigma} - Dh_2\hat{V}\left[v_1\frac{\partial}{\partial \xi}\left(\frac{J}{h_1}\right) - u_1\frac{\partial}{\partial \eta}\left(\frac{J}{h_2}\right) + Jf\right] - Dh_2u_1v_1\frac{\partial}{\partial \xi}\left(\frac{h_3}{h_1h_2}\right) = \\ -h_2gD\frac{\partial \zeta}{\partial \xi} + \frac{gh_2D}{\rho_0}\frac{\partial D}{\partial \xi}\int_\sigma^0 \sigma\frac{\partial \rho}{\partial \sigma}d\sigma - \frac{gh_2D^2}{\rho_0}\frac{\partial}{\partial \xi}\int_\sigma^0 \rho d\sigma + \frac{1}{D}\frac{\partial}{\partial \sigma}\left(K_m\frac{\partial Ju_1}{\partial \sigma}\right) + DJF_x\end{aligned} \quad (1)$$

$$\begin{aligned}\frac{\partial DJv_1}{\partial t} + \frac{\partial DJ\hat{U}v_1}{\partial \xi} + \frac{\partial DJ\hat{V}v_1}{\partial \eta} + \frac{\partial J\omega v_1}{\partial \sigma} - Dh_1\hat{U}\left[v_1\frac{\partial}{\partial \xi}\left(\frac{J}{h_1}\right) - u_1\frac{\partial}{\partial \eta}\left(\frac{J}{h_2}\right) + Jf\right] - Dh_1u_1v_1\frac{\partial}{\partial \eta}\left(\frac{h_3}{h_1h_2}\right) = \\ -h_1gD\frac{\partial \zeta}{\partial \eta} + \frac{gh_1D}{\rho_0}\frac{\partial D}{\partial \xi}\int_\sigma^0 \sigma\frac{\partial \rho}{\partial \sigma}d\sigma - \frac{gh_1D^2}{\rho_0}\frac{\partial}{\partial \eta}\int_\sigma^0 \rho d\sigma + \frac{1}{D}\frac{\partial}{\partial \sigma}\left(K_m\frac{\partial Jv_1}{\partial \sigma}\right) + DJF_v\end{aligned} \quad (2)$$

and the continuity equation is as follows:

$$\frac{\partial \zeta}{\partial t} + \frac{1}{J}\left[\frac{\partial}{\partial \xi}(DJ\hat{U}) + \frac{\partial}{\partial \eta}(DJ\hat{V})\right] + \frac{\partial \omega}{\partial \sigma} = 0 \quad (3)$$

where:

$$\omega = w - \sigma\left(\hat{U}\frac{\partial D}{\partial \xi} + \hat{V}\frac{\partial D}{\partial \eta}\right) - \left[(1+\sigma)\frac{\partial \zeta}{\partial t} + \hat{U}\frac{\partial \zeta}{\partial \xi} + \hat{V}\frac{\partial \zeta}{\partial \eta}\right] \quad (4)$$

The conservation equations for salinity and temperature can be written as follows:

$$\frac{\partial DJS}{\partial t} + \frac{\partial DJ\hat{U}S}{\partial \xi} + \frac{\partial DJ\hat{V}S}{\partial \eta} + \frac{\partial J\omega S}{\partial \sigma} = \frac{1}{D}\frac{\partial}{\partial \sigma}\left(K_h\frac{\partial JS}{\partial \sigma}\right) + DJF_s \quad (5)$$

$$\frac{\partial DJ\theta}{\partial t} + \frac{\partial DJ\hat{U}\theta}{\partial \xi} + \frac{\partial DJ\hat{V}\theta}{\partial \eta} + \frac{\partial J\omega \theta}{\partial \sigma} = \frac{1}{D}\frac{\partial}{\partial \sigma}\left(K_h\frac{\partial J\theta}{\partial \sigma}\right) + DJF_\theta \quad (6)$$

where $D = H + \zeta$, H is the mean water depth and ζ is the sea-surface elevation; u_1 and v_1 are the velocities defined at the directions of ξ and η; h_1, h_2, and h_3 are metric factors: $h_1 = \sqrt{x_\xi{}^2 + y_\xi{}^2}$, $h_2 = \sqrt{x_\eta{}^2 + y_\eta{}^2}$, and $h_3 = y_\xi y_\eta + x_\xi x_\eta$; J is the Jacobian function, $J = x_\xi y_\eta - x_\eta y_\xi$; $\hat{U} = \frac{1}{J}\left(h_2u_1 - \frac{h_3}{h_1}v_1\right)$, $\hat{V} = \frac{1}{J}\left(h_1v_1 - \frac{h_3}{h_2}u_1\right)$; f is the Coriolis parameter; g is the gravitational acceleration; K_h and K_m are the vertical-eddy-diffusion and -viscosity coefficients; F_ξ, F_η, F_S, and F_θ represent the horizontal-momentum, salt, and thermal-diffusion terms.

The numerical method of the model involves one-step-forward time discretization and the central spatial difference. The vertical-turbulent-vortex and viscous-diffusion terms, and the equation of the water level that causes extent gravity waves, are treated with implicit schemes. This model utilizes a third-order accurate HSIMT-TVD (high-order spatial interpolation at the middle temporal level coupled with a total-variation-diminishing scheme limiter) scheme to treat the advection terms in the salinity equation, effectively mitigating numerical dispersion and reducing numerical dissipation [38].

The domain of the model covers the Changjiang Estuary, Hangzhou Bay, and the adjacent sea, spanning from 117.5° E to 125° E longitude and from 27.5° N to 33.7° N latitude (Figure 2). The grid dimensions are 337 × 225 in the ξ and η directions, and there are 10 uniform layers in the vertical σ coordinate to better capture the estuarine terrain. Within the estuary, the grid resolutions range from 100 to 500 m. The smallest grid spacing near the bifurcation of the NB and SB is approximately 100 m, facilitating more accurate modeling of the saltwater spillover from the NB. Outside the estuary, the minimum grid resolution is approximately 10 km. The model grids exhibit good orthogonality and smoothness, accurately fixing the shape of the coast near the bifurcation and the deep-water navigation project.

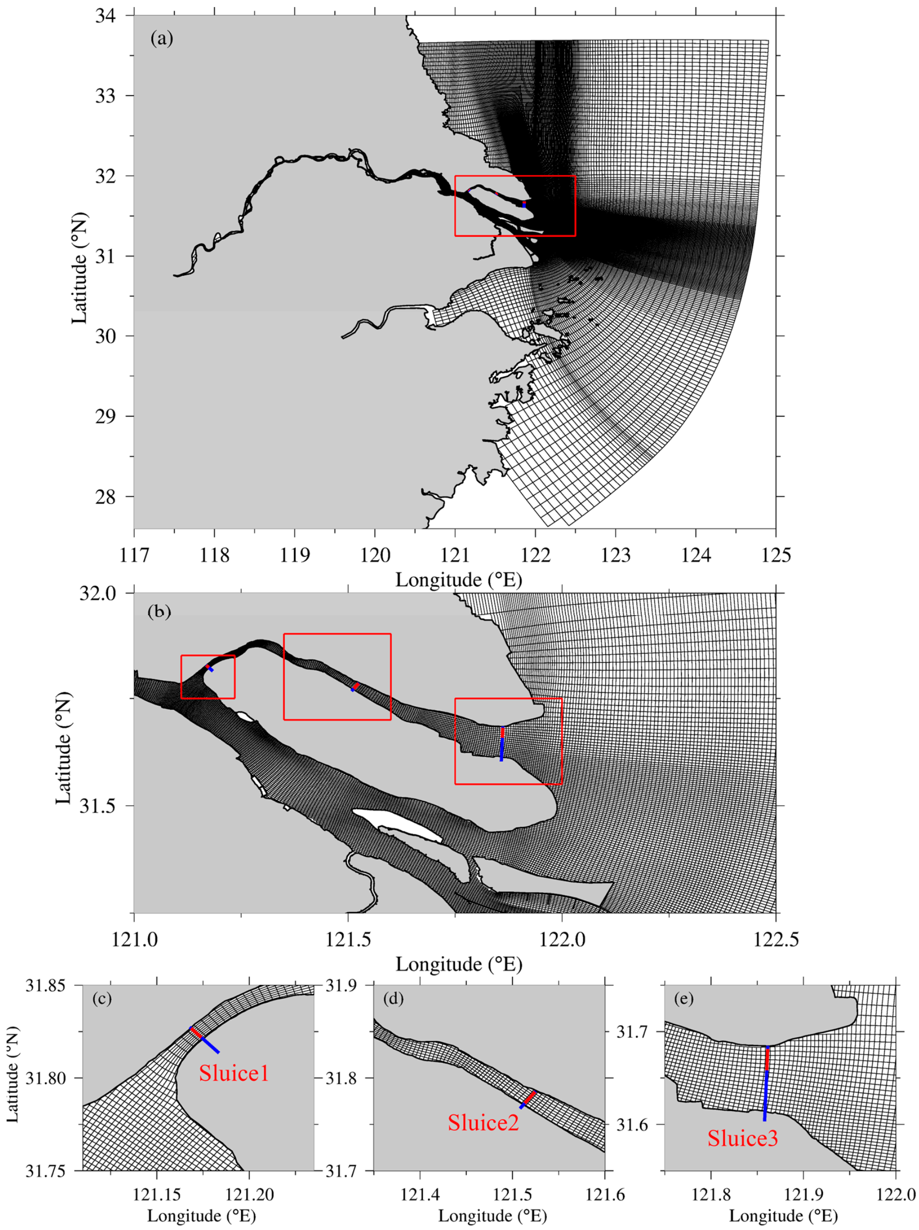

Figure 2. Numerical-model grid (**a**). Enlarged views of the model grid around the locations of the three sluices (**b**). The structures of sluice 1 (**c**), sluice 2 (**d**), and sluice 3 (**e**).

The open-sea boundary conditions are driven by tidal elevations, composing the harmonic constants of the 15 tidal constituents (M_2, S_2, N_2, K_2, K_1, O_1, P_1, Q_1, MF, MM, MN_4, M_4, MS_4, S_1, $2N_2$), which are from the TPXO dataset (https://www.tpxo.net/otps, accessed on 10 July 2023) [39]. The initial salinity field was taken from the *Ocean Atlas in Huanghai Sea and East China Sea (Hydrology)* [40]. The upstream river discharge boundary condition is based on data measured at the Datong Hydrological Station. The wind data are sourced from the European Centre for Medium-Range Weather Forecasts (ECMWF, https://cds.climate.copernicus.eu, accessed on 10 July 2023), with a spatial resolution of 0.5° × 0.5° and a temporal resolution of 6 h. The water depth was measured for the entire Changjiang Estuary in 2021. The time step is variable, and the calculation formula is as follows:

$$\text{Time step} = 0.85 \times Min\left[\left(\frac{\Delta x}{u}\right)_{i=1,n}, \left(\frac{\Delta y}{v}\right)_{i=1,n}\right] \quad (7)$$

The CPU we used was an 11th Gen Intel (R) Core(TM) i7-11700K @ 3.60 GHz. The CPU time required for each simulation of 90 d was approximately 6 h.

2.2. Model Validation

To demonstrate the model capacity, the field-measured data in the NB from 15 to 26 April 2023 were used to validate the model. Three observation sites (A, B, and C) were located in the NB from the upper to the lower reaches (Figure 1). Tripods were placed on the riverbed to acquire continuous data of the current velocity and direction profile with an acoustic Doppler current profiler (ADCP), and of the water level, salinity, and water temperature with conductivity–temperature–depth (CTD) for approximately 33 h at each site. The correlation coefficient (CC), root-mean-square error (RMSE), skill score (SS), and Nash–Sutcliffe efficiency (NSE) were used to quantify the validation [41–43].

The results of the model validation are shown in Figure 3, and the skill assessments are summarized in Table 1. The water level elevations at the measured sites were well simulated, with high CCs (>0.98), low RMSEs (<0.20 m), excellent SSs (>0.99), and excellent NSEs (>0.95). In terms of the velocity, the CCs all exceeded 0.70. Furthermore, the SSs were above 0.82 and the NSEs were greater than 0.42 at each site. In terms of the salinity, the CCs all exceeded 0.83. Furthermore, the SSs were above 0.86 and the NSEs were greater than 0.25 at each site. These results mean that the model performance was very good. Therefore, the results of the model validation indicate that the model can successfully simulate the variation processes in elevation, current, and salinity.

Table 1. CCs, RMSEs, SSs, and NSEs of the elevation, velocity, and salinity at measured sites A, B, and C (value in the surface layer/value in the bottom layer).

	Site	CC	RMSE	SS	NSE
Elevation	A	0.98	0.20	0.99	0.95
	B	0.99	0.17	0.99	0.98
	C	0.99	0.18	0.99	0.98
Velocity	A	0.82/0.83	0.21/0.09	0.90/0.90	0.68/0.57
	B	0.88/0.75	0.26/0.18	0.93/0.84	0.76/0.56
	C	0.74/0.70	0.33/0.16	0.85/0.82	0.52/0.42
Salinity	A	0.88/0.88	0.02/0.01	0.86/0.93	0.33/0.75
	B	0.90/0.98	1.29/0.61	0.92/0.99	0.60/0.95
	C	0.83/0.95	1.07/0.84	0.87/0.97	0.25/0.89

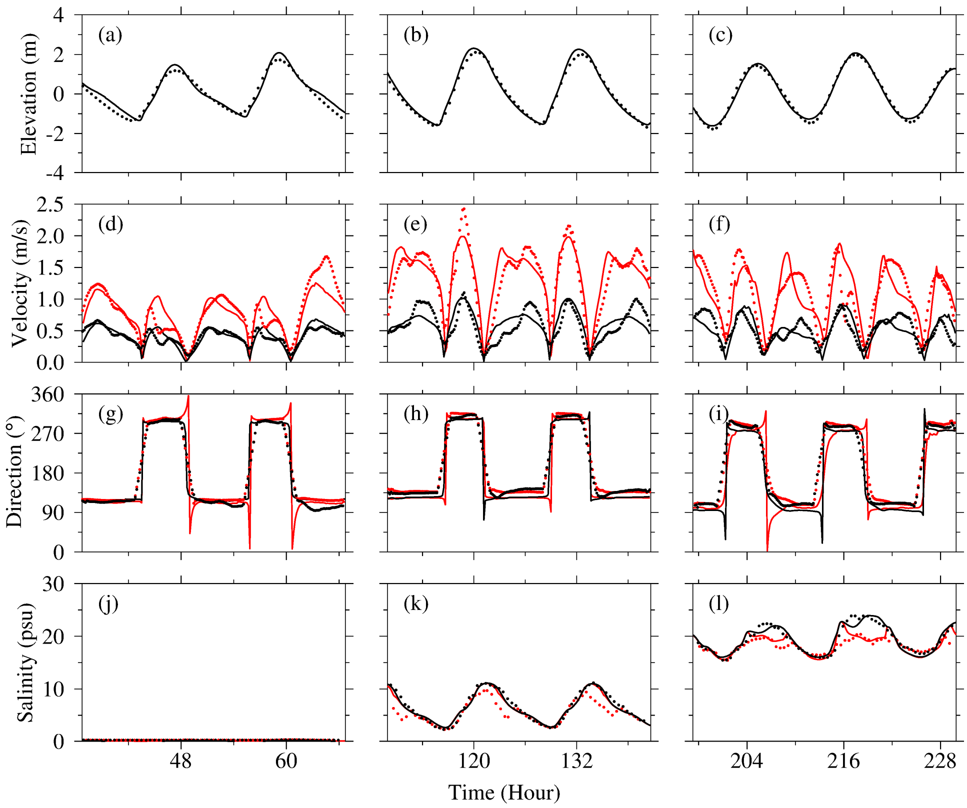

Figure 3. Comparison between the modeled (lines) and observed (dots) elevation (**a**–**c**), current velocity (**d**–**f**), current direction (**g**–**i**), and salinity (**j**–**l**) at measured sites A (left panel), B (middle panel), and C (right panel). Red indicates the surface layer, and black indicates the bottom layer.

2.3. Numerical Experimental Design

As mentioned above, the most severe saltwater intrusion event in the Changjiang Estuary during the dry season over the last 30 years occurred in February 2014. This intrusion cut off the freshwater input for 23 days into the QCSR, creating a serious threat to the water safety in Shanghai. Zhu et al. [5] revealed that the extremely severe saltwater intrusion was caused by persistent and strong northerly winds. In this paper, this severe saltwater intrusion event was taken as the scenario to analyze the effects of sluices at different locations in the NB on the saltwater intrusion and freshwater resources.

Persistent and strong northerly winds on 6–14 February 2014, lasting 9 days, with an average wind speed of 10.01 m/s and a maximum wind speed of 17.6 m/s on 10 February, were recorded at the weather station on the Chongming Eastern Shoal (location is shown in Figure 1, WS) (Figure 4a,b). After a two-day southerly wind on 15–16 February, there was a four-day strong northerly wind on 17–20 February 2014. The observed data indicated that persistent and strong northerly winds occurred. The wind data from the ECMWF had the same characteristic [5], which was used to drive the model in this paper.

A total of 4 numerical experiments were designed. EX0 is the experiment without sluice construction, and EX1, EX2, and EX3 are the experiments with sluice 1, sluice 2, and sluice 3 construction, respectively. The operation modes of the sluices in EX1, EX2, and EX3 are all set to closed during the flood currents and to opened during the ebb currents. The designed sluices, sluice 1, sluice 2, and sluice 3, are in the upper, middle, and lower reaches of the NB, respectively (Figure 1). The Changjiang Estuary has a semidiurnal tide and two flood currents daily. The sluices are closed during flood currents to prevent saltwater transport upstream. They are opened during ebb currents to facilitate the navigation of vessels. The sluices are closed when the downstream elevation is 1 mm higher than the upstream elevation and the flood current velocity is greater than 1 cm/s. The sluices are opened when the upstream elevation is 3 mm higher than the downstream elevation.

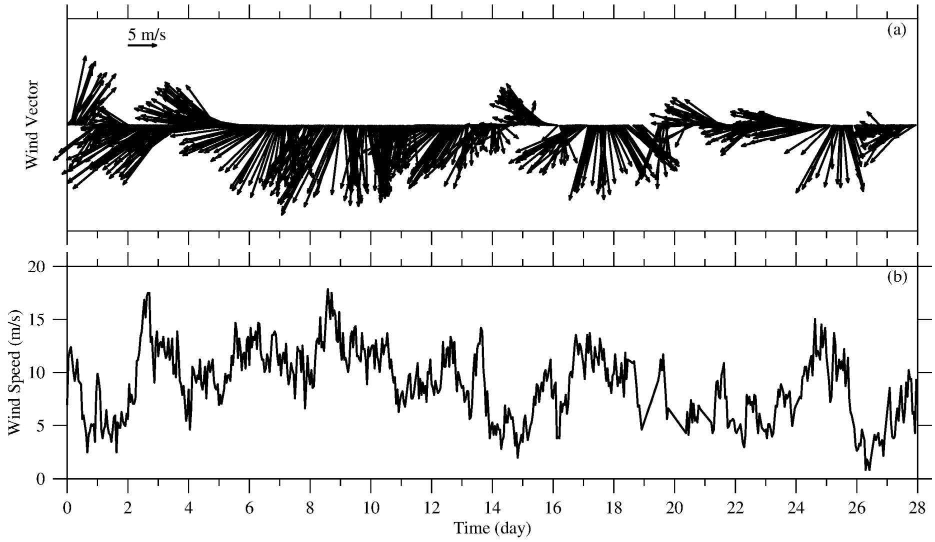

Figure 4. Temporal variations in the wind vector (**a**) and wind speed (**b**) at WS in February 2014.

3. Results

3.1. Saltwater Intrusion before Sluice Construction

During the neap tide (from 5:00 on 7 February to 9:30 on 10 February 2014 in EX2, and the same hereinafter), under the force of low river discharge and persistent, strong northerly winds in the dry season (Figure 4), most areas of the SB were covered by saline water, and freshwater appeared only along the coast of the upper and middle SB, meaning that the saltwater intrusion was very severe (Figure 5a). The net transect water flux (NTWF), WDR, and net transect salt flux (NTSF) across S1 in the upper reaches of the NB (position shown in Figure 1a) were −46 m^3/s, −0.4%, and −2 kg/s, respectively, as shown in Tables 2 and 3 (the negative sign means the upstream transport of water and salt, and the same hereinafter). The entire NB was occupied by highly saline water, and a small fraction of the saltwater was transported to the SB, producing saltwater spillover from the NB into the SB. Driven by the persistent, strong northerly winds, the NTWF, WDR, and NTSF across S3 in the upper reaches of the NC were −1331 m^3/s, −10.9%, and −19 kg/s, respectively. The water in the SC, North Passage, and South Passage flowed into the sea. The saltwater intrusion was more severe in the South Passage than in the North Passage.

Table 2. The NTWF and WDR across S1, S2, S3, and S4 in the upper reaches of the NB, SB, NC, and SC, respectively, during spring and neap tides.

Project	**NTWF (m^3/s)**				**WDR (%)**			
	Spring		**Neap**		**Spring**		**Neap**	
	NB	**SB**	**NB**	**SB**	**NB**	**SB**	**NB**	**SB**
EX0	−537	11,453	−46	11,995	−4.9	104.9	−0.4	100.4
EX1	678	10,209	834	11,176	6.2	93.8	6.9	93.1
EX2	3880	7196	2327	9774	35.1	64.9	19.2	80.8
EX3	3984	7274	1826	10,145	35.4	64.6	15.2	84.8
	NC	SC	NC	SC	NC	SC	NC	SC
EX0	7492	3715	−1331	13,596	66.9	33.1	−10.9	110.9
EX1	6870	3053	−2057	13,517	69.2	30.8	−18.0	118.0
EX2	4559	2355	−3065	13,135	65.9	34.1	−30.4	130.4
EX3	4823	2171	−3068	13,476	69.0	31.0	−29.5	129.5

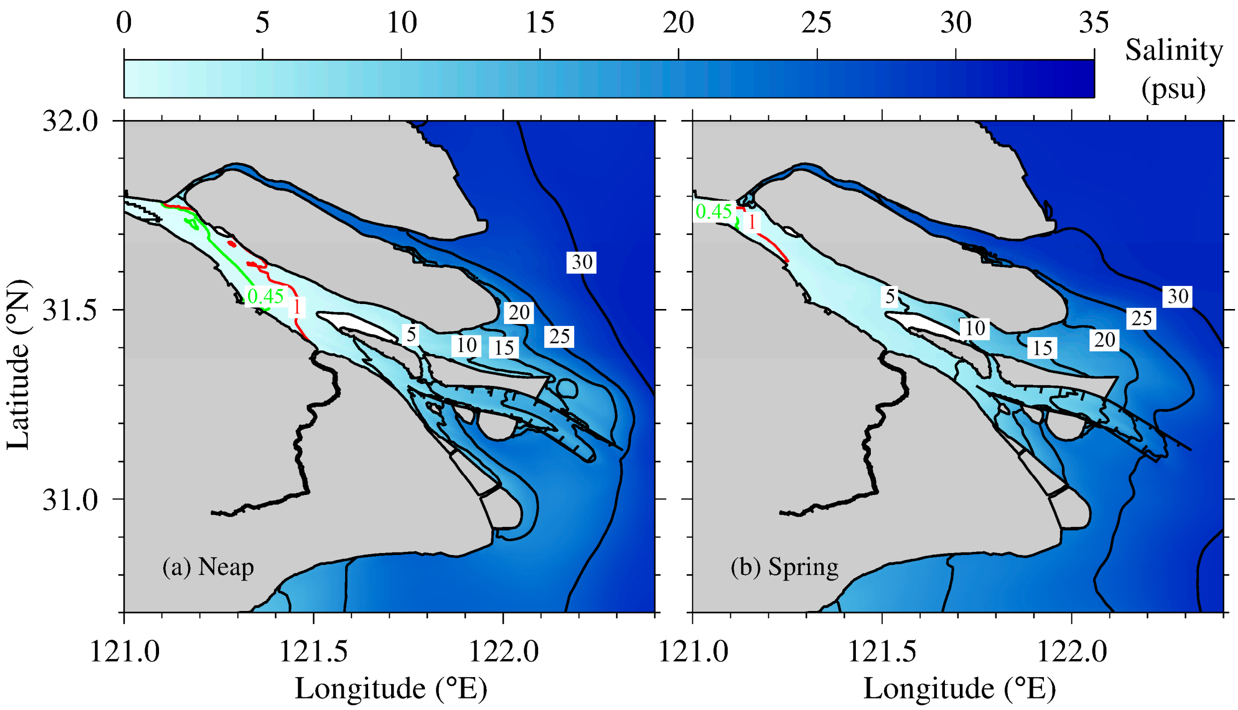

Figure 5. Distributions of the tidally and vertically averaged salinity during neap (**a**) and spring (**b**) tides in EX0.

During the spring tide (from 13:00 on 15 February to 14:00 on 18 February 2014 in EX2, and the same hereinafter), the saltwater intrusion increased as the tidal power increased. The NTWF, WDR, and NTSF across S1 in the upper reaches of the NB were -537 m^3/s, -4.9%, and -13 kg/s, respectively. The enhanced saltwater spillover from the NB reduced the freshwater area in the upper reaches of the SB (Figure 5b). The northerly wind weakened during the spring tide, and the NC became the main channel for the water discharge into the sea. The NTWF, WDR, and NTSF across S3 in the upper reaches of the NC were 7492 m^3/s, 66.9%, and 37 kg/s, respectively. Simultaneously, the enhanced tidal mixing weakened the salinity front in the NC, resulting in a decrease in the landward baroclinic pressure gradient force and a significant increase in the WDR in the NC, which far exceeded that in the SC. Similar to that during the neap tide, the saltwater intrusion in the South Passage was more severe than that in the North Passage.

Table 3. The NTSF across S1, S2, S3, and S4 in the upper reaches of the NB, SB, NC, and SC, respectively, during spring and neap tides.

Project	NTSF (kg/s)			
	Spring		Neap	
	NB	SB	NB	SB
EX0	−13	14	−2	2
EX1	0	0	0	0
EX2	1	−1	0	0
EX3	1	−1	0	0
	NC	SC	NC	SC
EX0	37	10	−19	13
EX1	33	7	−24	8
EX2	27	10	−25	16
EX3	29	8	−28	17

3.2. Distributions of Elevation and Current after Sluice Construction

Figure 6 displays the variations in the elevation and current velocity at points F and G (shown in Figure 1) in EX2. Driven by the barotropic force, the current flowed downstream through sluice 2 when the sluice was opened, the elevation upstream of the sluice was much higher than that downstream of the sluice, and no water flux crossed the sluice when the sluice was closed. This operation mode of the sluice completely cut off the upstream saltwater intrusion, and a large amount of water upstream of the sluice was pumped into the area downstream of the sluice, greatly changing the WDR between the NB and SB. The situations at points D and E upstream and downstream of sluice 1 and at points H and I upstream and downstream of sluice 3 were similar to those in Figure 6, so the figures are omitted.

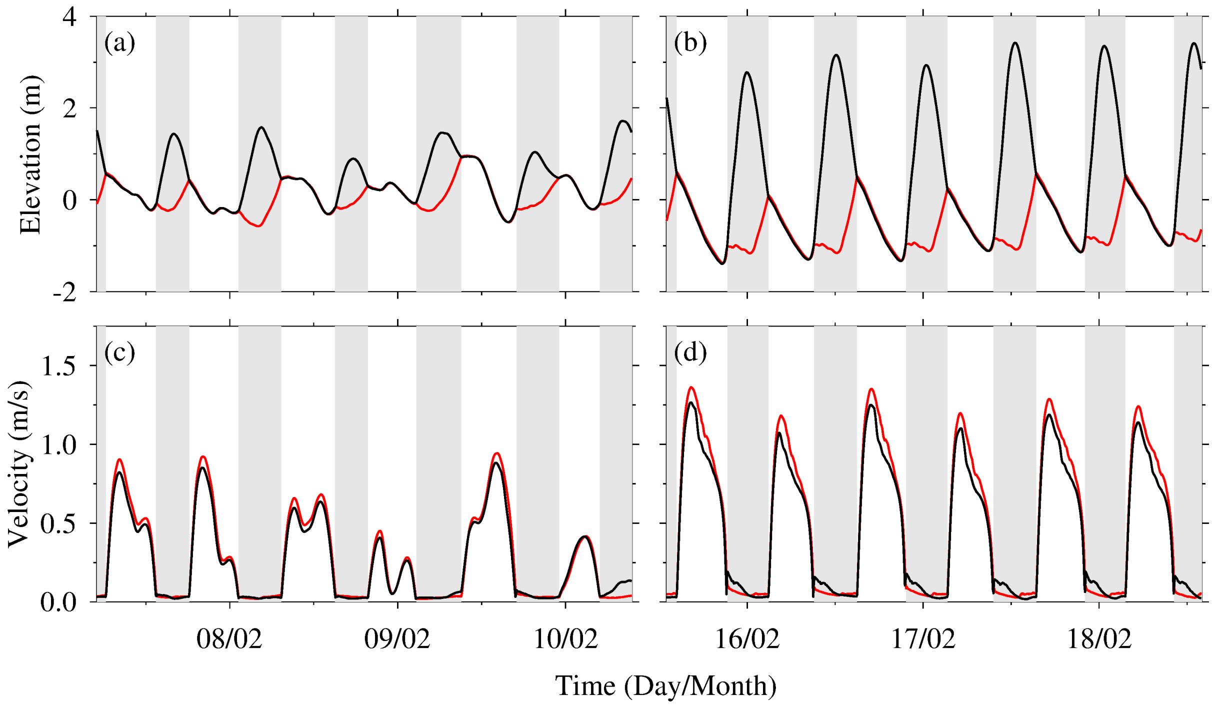

Figure 6. Temporal variations in elevation (**a**,**b**) and vertically averaged current velocity (**c**,**d**) at site F (red) and site G (black) during neap (left) and spring (right) tides in EX2. Gray bars indicate the periods when the sluice was closed.

At the maximum flood current (at 14:00, 12:00, and 11:00 on 17 February 2014 for sluices 1, 2, and 3, respectively) (Figure 7), before the sluices were built, the flood current flowed upstream with maximum current velocities of 1.5, 2.0, and 1.2 m/s at the locations of sluices 1, 2, and 3, respectively. After the sluices were built, the sluices were closed during the flood current, resulting in distinct decreases in the flood current upstream and downstream of the sluices. There appeared to be counterflow downstream of sluice 3 due to the water convergence induced by the blocking of the flood current.

At the maximum ebb current (at 18:00, 16:00, and 15:00 on 17 February 2014 for sluices 1, 2, and 3, respectively) (Figure 8), before the sluices were built, the ebb current flowed downstream at the locations of sluices 1, 2, and 3. After the sluices were built, the sluices were open during the ebb current; therefore, the ebb current is nearly the same as before the sluices were built upstream and downstream of the sluices. Downstream of sluice 3, the current direction is reversed on the north side and enhanced on the south side.

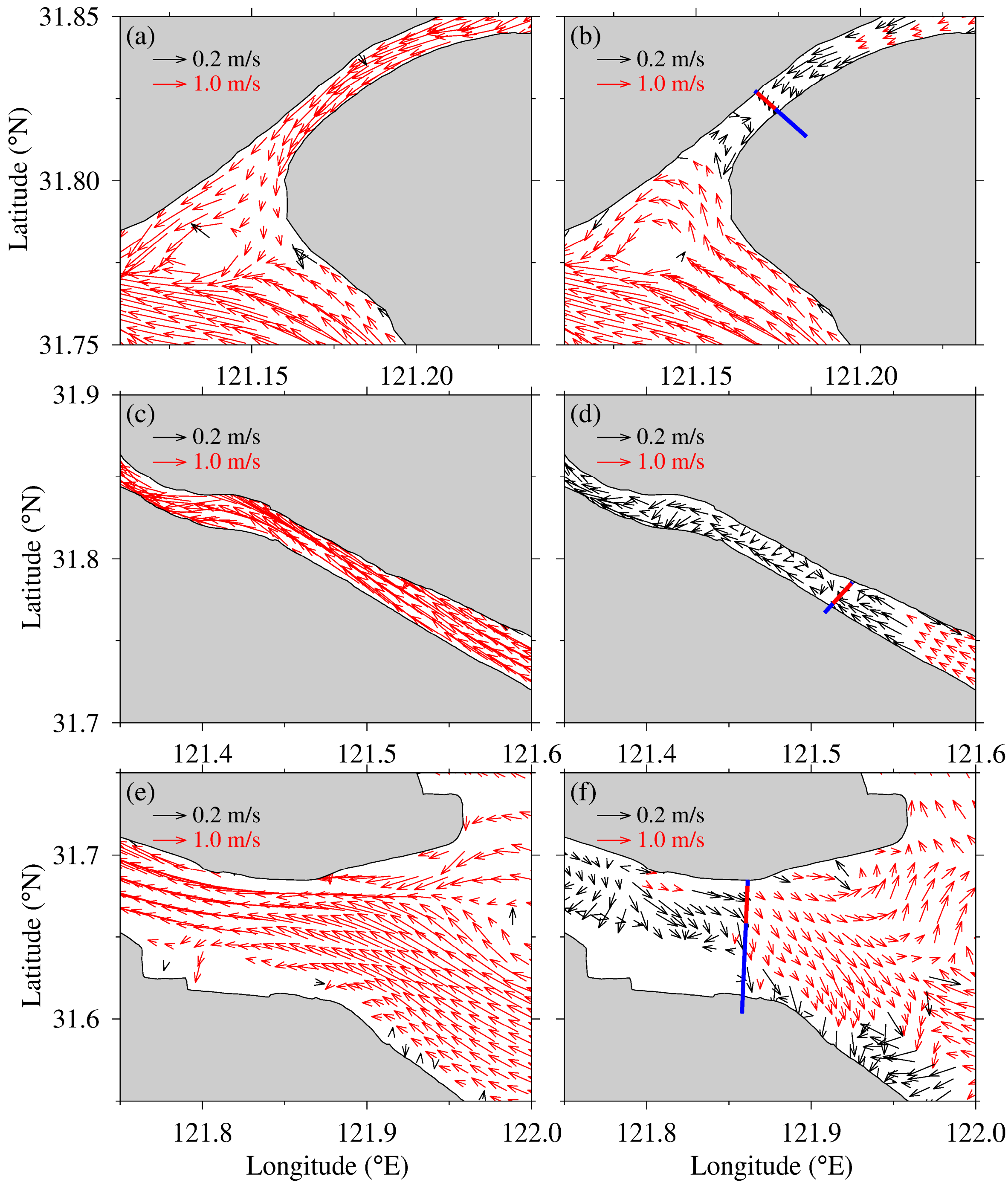

Figure 7. Modeled surface currents in the upper (**a**,**b**), middle (**c**,**d**), and lower (**e**,**f**) reaches of the NB at the maximum flood in EX0 (**a**,**c**,**e**), EX1 (**b**), EX2 (**d**), and EX3 (**f**). Left panel: before the sluices; right panel: after the sluices.

The residual unit width water flux was adopted to better explain the water transport after sluice construction [41]. Due to the operation mode of the sluice, the net water transport was seaward across the sluices and larger during the spring tide than during the neap tide (Figure 9). For sluice 3, the residual unit width water flux flowed into the river mouth along the north coast and flowed out of the river mouth along the south coast during the neap tide, driven by the persistent northerly north winds; however, during the spring tide, it flowed southeastward after leaving the sluice and then flowed northeastward due to larger tidal Stokes and pumping transport [42].

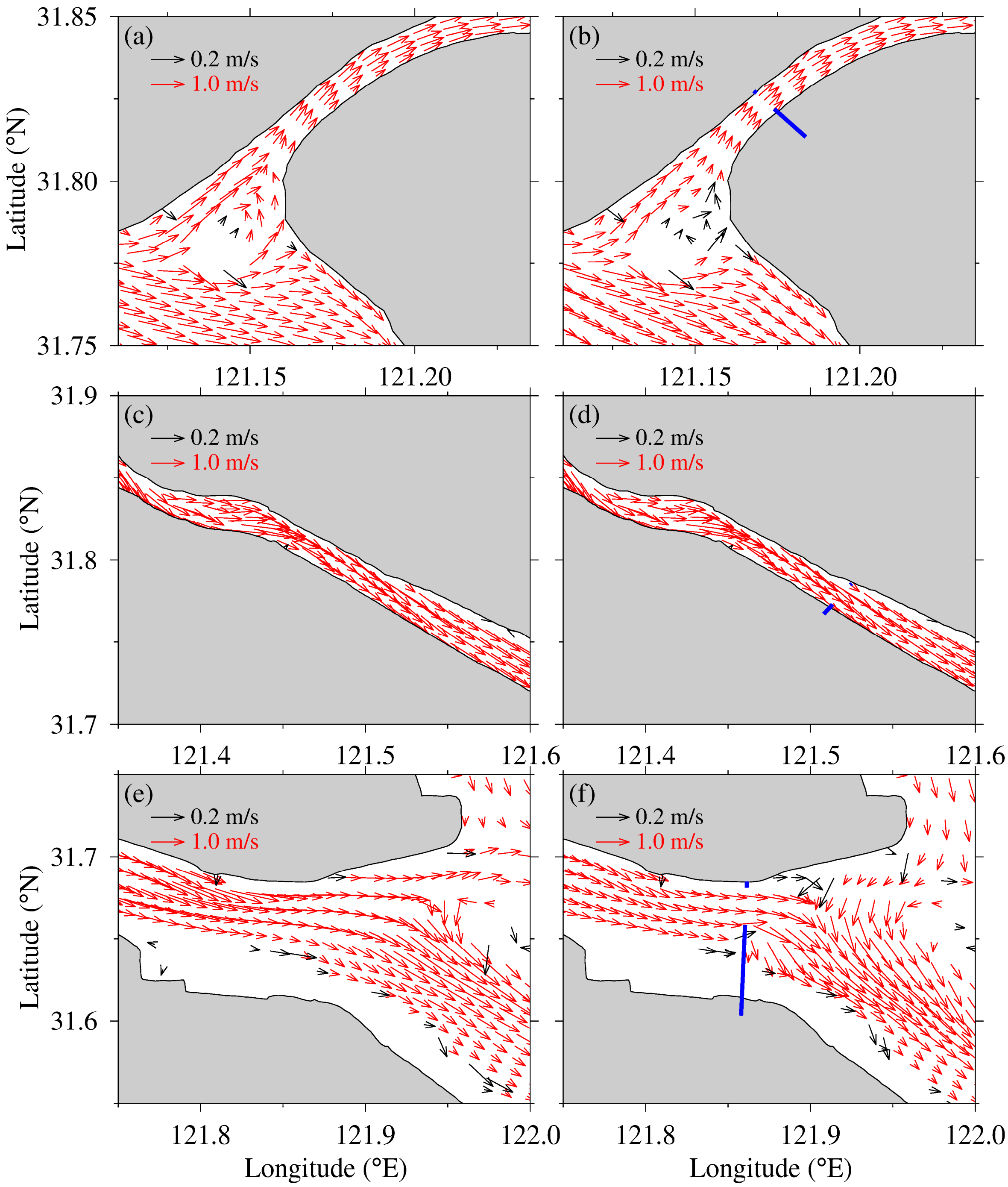

Figure 8. Modeled surface currents in the upper (**a**,**b**), middle (**c**,**d**), and lower (**e**,**f**) reaches of the NB at the maximum ebb in EX0 (**a**,**c**,**e**), EX1 (**b**), EX2 (**d**), and EX3 (**f**). Left panel: before the sluices; right panel: after the sluices.

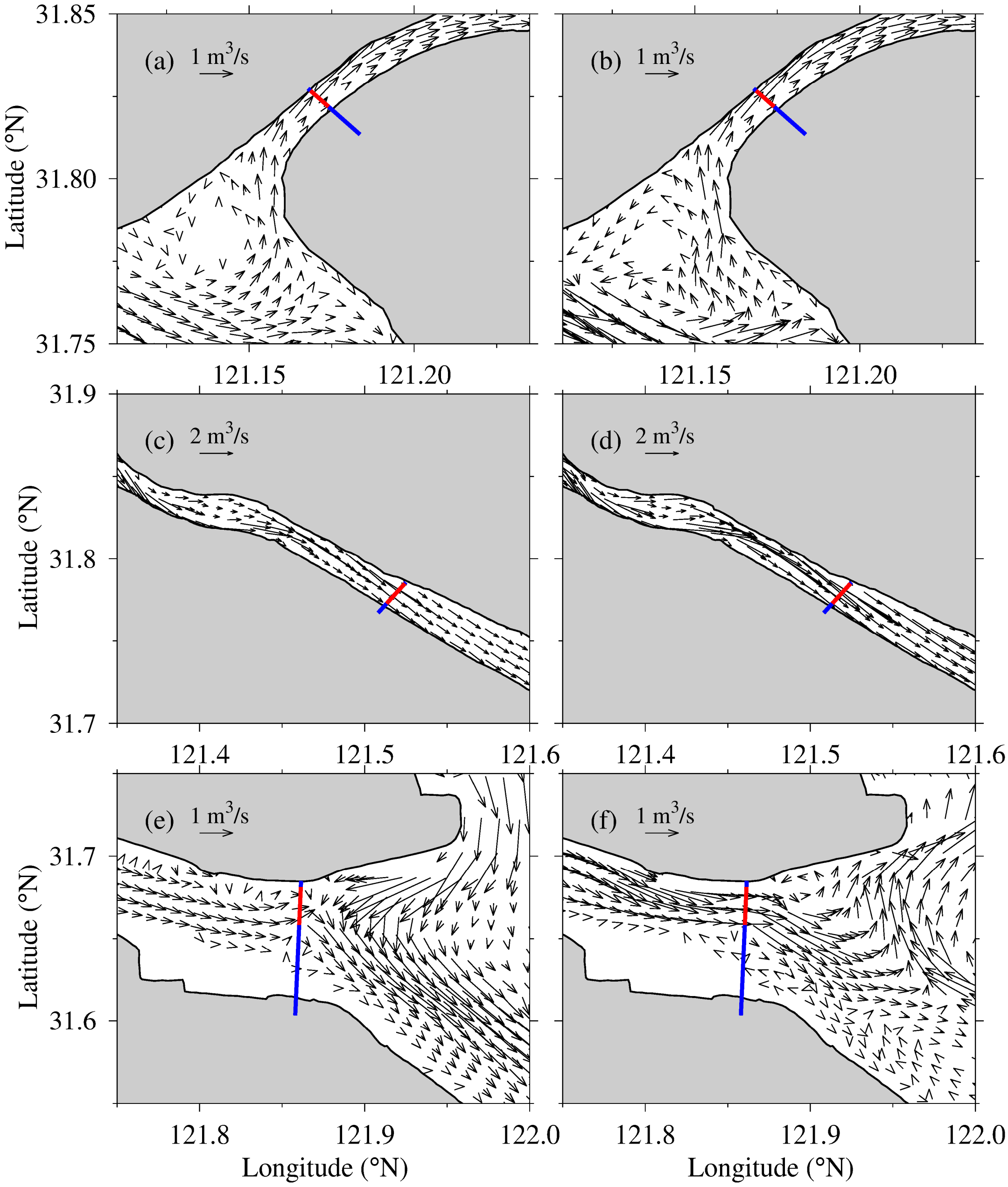

Figure 9. Distributions of residual unit width water flux during the neap tide (**left**) and the spring tide (**right**) in EX1 (**a**,**b**), EX2 (**c**,**d**), and EX3 (**e**,**f**).

3.3. Saltwater Intrusion after Sluice Construction

After the construction of sluice 1 in EX1, during the neap tide (Figure 10a,c), the NTWF, WDR, and NTSF across S1 were −834 m^3/s, −6.9%, and 0 kg/s, respectively (Tables 2 and 3). Moreover, the NTWF, WDR, and NTSF across S2 were −11,176 m^3/s, 93.1%, and 0 kg/s, respectively. Compared to EX0, the WDR across S1 increased by 7.3%, resulting in a noticeable increase in the inflow of water into the NB and the disappearance of saltwater spillover from the NB into the SB. The salinity in the NB significantly decreased, with a maximum of 15.0 psu. The freshwater area in the upper reaches of the SB expanded, and the 0.45 psu isohaline shifted toward the lower reaches of the SB. The water entering the SB decreased, intensifying the saltwater intrusion in the NC. There was still landward seawater transport from the NC into the SC around western Changxing Island. There was no significant change in the seaward NTWF in the SC. The NTWF, WDR, and NTSF across S3 were −2057 m^3/s, −18%, and −24 kg/s, respectively. Moreover, the NTWF, WDR, and

NTSF across S4 were 13,517 m^3/s, 118%, and 8 kg/s, respectively. Thus, an increase in salinity occurred in the NC, with a maximum value of approximately 5.0 psu. The north dike of the Deep Water Way obstructed the southward transport of saltwater under a strong northerly wind. The reduction in seaward runoff in the NC further raised the salinity on the north side of the dike in the NC. The salinity in the upper reaches of the North Passage, middle reaches, and southern side of the lower reaches of the South Passage decreased.

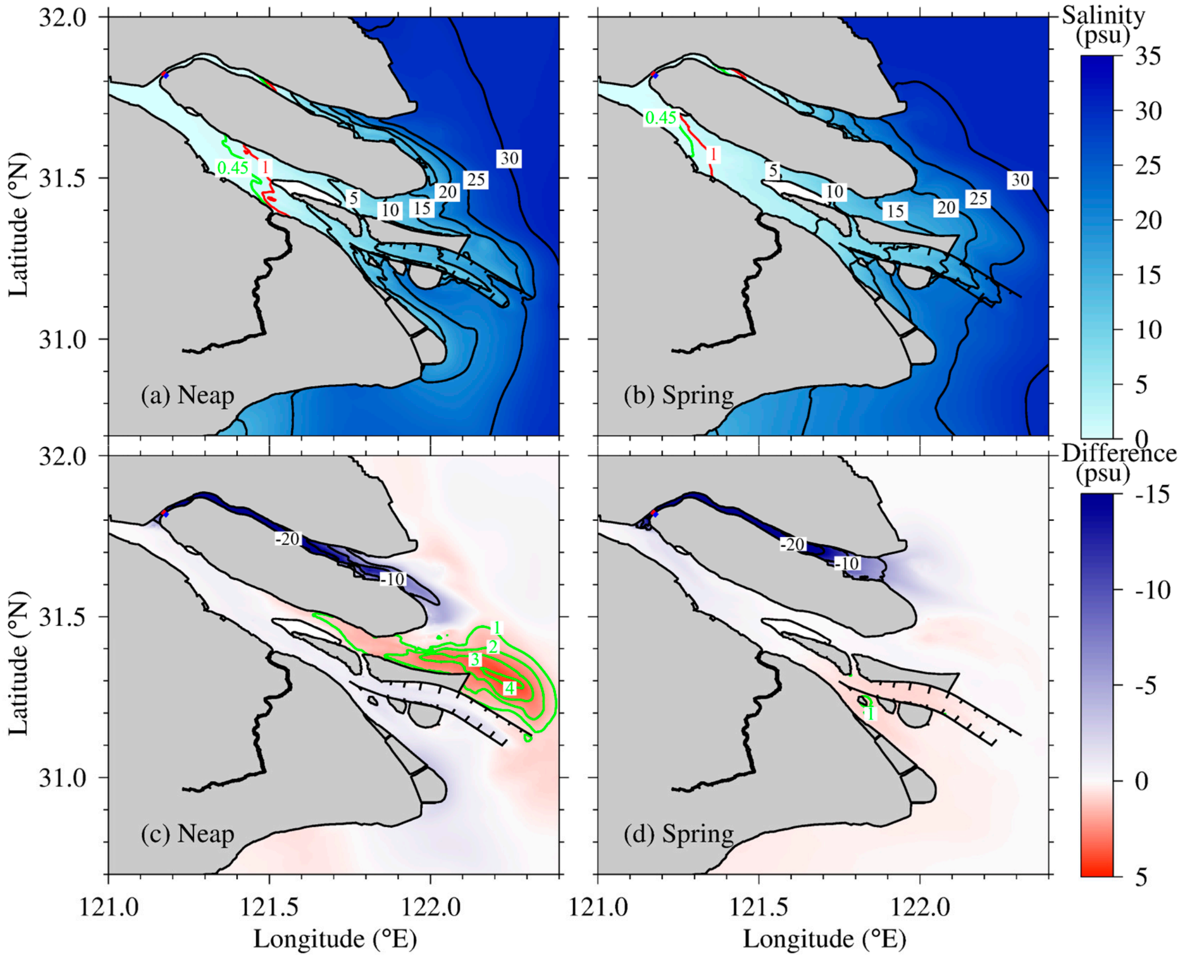

Figure 10. Distributions of the tidally and vertically averaged salinity in EX1 (**a**,**b**) and their difference between EX1 and EX0 (**c**,**d**) during neap (**left**) and spring (**right**) tides.

After the construction of sluice 2 in EX2 (Figure 11), during the neap tide in EX2 (Figure 11a,c), the NTWF, WDR, and NTSF across S1 were 2327 m^3/s, 19.2%, and 0 kg/s, respectively. Moreover, the NTWF, WDR, and NTSF across S2 were 9774 m^3/s, 80.8%, and 0 kg/s, respectively. Compared to EX0, the WDR across S1 increased by 19.6%, resulting in the disappearance of saltwater spillover from the NB. The entire upper reaches of the NB became a freshwater area, and the isohalines in the lower reaches of the NB shifted outward. The freshwater area in the upper reaches of the SB expanded with the 0.45 psu and 1.0 psu isohalines moving seaward. Due to the inflow of water into the NB, the runoff transported seaward in the SB decreased. More landward seawater was transported from the NC and entered the SC. The NTWF, WDR, and NTSF across S3 were −3065 m^3/s, −30.4%, and −25 kg/s, respectively. Moreover, the NTWF, WDR, and NTSF across S4 were 13,135 m^3/s, 130.4%, and 16 kg/s, respectively. The salinity in the upper reaches of the NC, entire SC, North Passage, and South Passage increased with the decrease in runoff in these channels. In the lower reaches of the NC, the salinity distinctly decreased, which was caused by less saline water in the river mouth of the NB flowing southward on the east side of Chongming Island and reaching the river mouth of the NC, driven by the strong northerly wind.

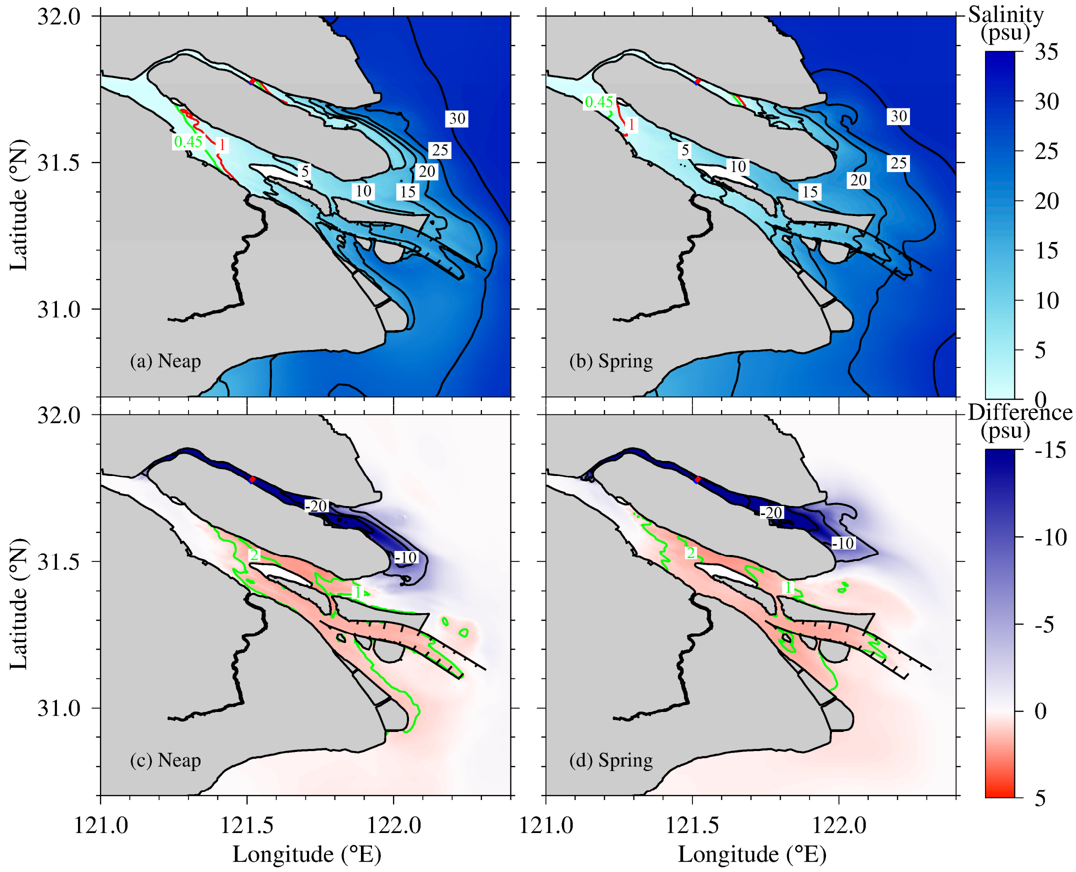

Figure 11. Distributions of the tidally and vertically averaged salinity in EX2 (**a**,**b**) and their difference between EX2 and EX0 (**c**,**d**) during neap (**left**) and spring (**right**) tides.

After the construction of sluice 3 in EX3, during the neap tide in EX3 (Figure 12a,c), the NTWF, WDR, and NTSF across S1 were 1826 m^3/s, 15.2%, and 0 kg/s, respectively. Moreover, the NTWF, WDR, and NTSF across S2 were 10,145 m^3/s, 84.8%, and 0 kg/s, respectively. Compared to EX0, the WDR across S1 increased by 15.6%, resulting in the complete disappearance of saltwater spillover from the NB. The upper and middle reaches of the NB became entirely freshwater areas. The salinity in the NC, SC, North Passage, and South Passage increased, with a maximum value of more than 2.0 psu, due to the reduced runoff in the SB. There was a reduction in salinity in the lower northern reaches of the NC and east of the Chongming East Shoal due to the decreased salinity in the lower reaches of the NB.

During the spring tide (Figure 10b,d), the NTWF, WDR, and NTSF across S1 were -678 m^3/s, 6.2%, and 0 kg/s, respectively. Moreover, the NTWF, WDR, and NTSF across S2 were 10,209 m^3/s, 93.8%, and 0 kg/s, respectively. The freshwater area in the upper reaches of the NB expanded, leading to a significant decrease in salinity in the entire NB by more than 10.0 psu. The freshwater area in the upper reaches of the SB increased, resulting in a decrease in the salinity by approximately 1.0 psu. The NTWF, WDR, and NTSF across S3 were 6870 m^3/s, 69.2%, and 33 kg/s, respectively. Moreover, the NTWF, WDR, and NTSF across S4 were 3053 m^3/s, 30.8%, and 7 kg/s, respectively. Unlike the saltwater intrusion during the neap tide, more runoff entered the NC than the SC, leading to an increase in the saltwater intrusion in the North Passage and South Passage, causing the salinity to increase by 0.5–1.0 psu.

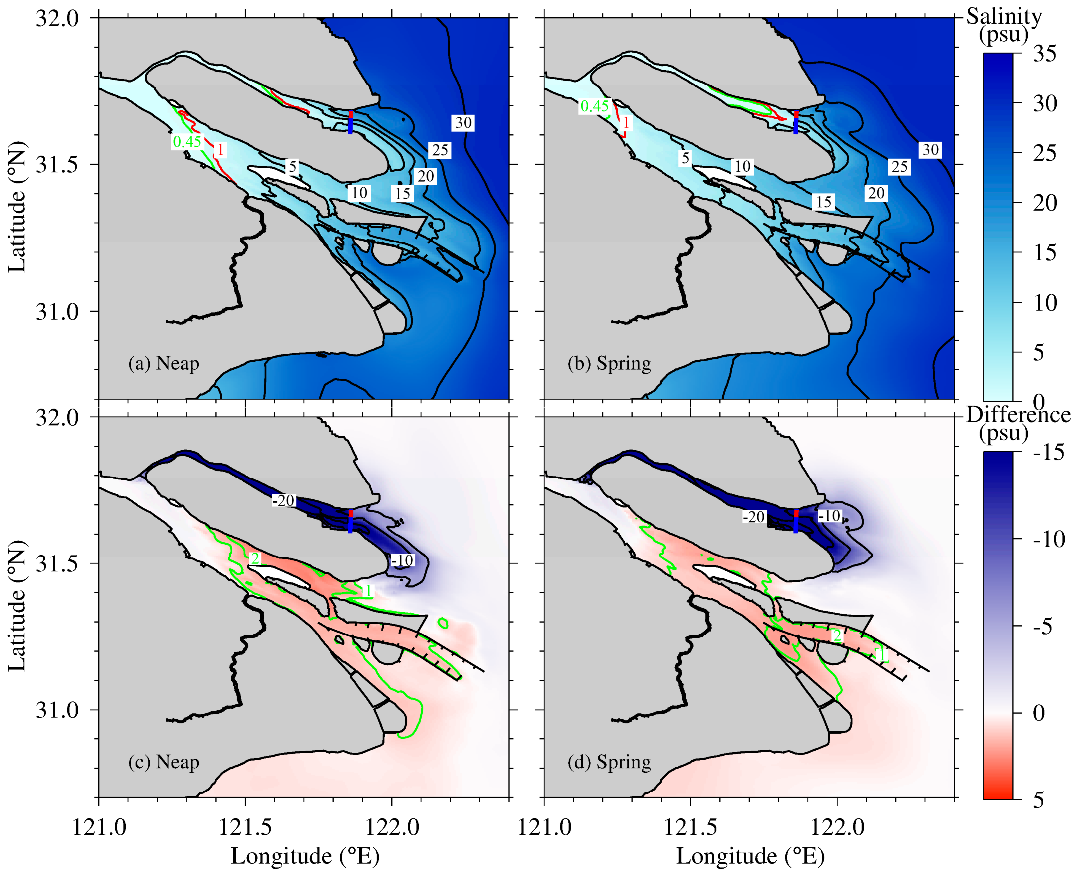

Figure 12. Distributions of the tidally and vertically averaged salinity in EX3 (**a**,**b**) and their difference between EX3 and EX0 (**c**,**d**) during neap (**left**) and spring (**right**) tides.

During the spring tide in EX2 (Figure 11b,d), the NTWF, WDR, and NTSF across S1 were 3880 m^3/s, 35.1%, and 1 kg/s, respectively. Moreover, the NTWF, WDR, and NTSF across S2 were 7196 m^3/s, 64.9%, and −1 kg/s, respectively. Compared to EX0, the WDR across S1 increased by 40%, resulting in a reduction in runoff entering the SB. Unlike the neap tide, the WDR and NTSF across S3 were 65.9% and 27 kg/s, respectively. The WDR and NTSF across S4 were 34.1% and 10 kg/s, respectively. Most of the runoff was transported seaward through the NC. However, because the NTWF across S2 in the SB decreased by nearly 4300 m^3/s, the salinity only decreased in the NB but increased in the NC, SC, North Passage, and South Passage.

During the spring tide in EX3 (Figure 12b,d), the NTWF, WDR, and NTSF across S1 were 3984 m^3/s, 35.4%, and 1 kg/s, respectively. Moreover, the NTWF, WDR, and NTSF across S2 were 7274 m^3/s, 64.6%, and −1 kg/s, respectively. Compared to EX0, the WDR across S1 increased by 40.3%, entirely eliminating the phenomenon of saltwater spillover from the NB. The upper and middle reaches in the NB had freshwater, and the salinity decreased in the upper reaches of the SB. The WDR and NTSF across S3 were 69% and 29 kg/s, respectively. The WDR and NTSF across S4 were 31% and 8 kg/s, respectively. The salinity decreased in the lower northern reaches of the NC. Additionally, the salinity in the North Passage and South Passage increased due to the decrease in runoff through the North Passage and South Passage.

3.4. Impact on Freshwater Resources

The Dongfeng Xisha Reservoir is located north of the upper reaches of the SB. It is one of the reservoirs influenced earliest by saltwater spillover from the NB. In EX0, severe saltwater spillover occurred. The surface salinity exceeded the drinking water salinity standard (0.45 psu) most of the time, reaching a maximum value of 2.5 psu (Figure 13a,b).

Periodic freshwater occurred due to the combined effects of runoff and tides. The surface salinity and the duration of the available freshwater intake time in February were 0.83 and 7.95 days, respectively. In EX1, occasional saltwater intrusion from the NC only occurred in mid-February. The sluice construction eliminated saltwater spillover from the NB. In February, the surface salinity at the water intake of the Dongfeng Xisha Reservoir decreased, with a maximum value of 2.0 psu. The surface salinity and the duration of the available water intake time in February were 0.09 and 26.72 days, respectively. Compared to EX0, the available water intake time increased by 18.77 days. In EX2, intermittent saltwater intrusion occurred in the early- and mid-February periods. However, the surface salinity distinctly decreased after sluice construction, except for the temporary increase in mid-February due to saltwater intrusion from the NC downstream. The surface salinity and the duration of the available water intake time in February were 0.24 and 23.57 days, respectively. Compared to EX0, the available water intake time increased by 15.62 days. In EX3, the salinity variations were similar to those in EX2. The surface salinity and the duration of the available water intake time in February were 0.24 and 23.28 days, respectively. Compared to EX0, the available water intake time increased by 15.33 days.

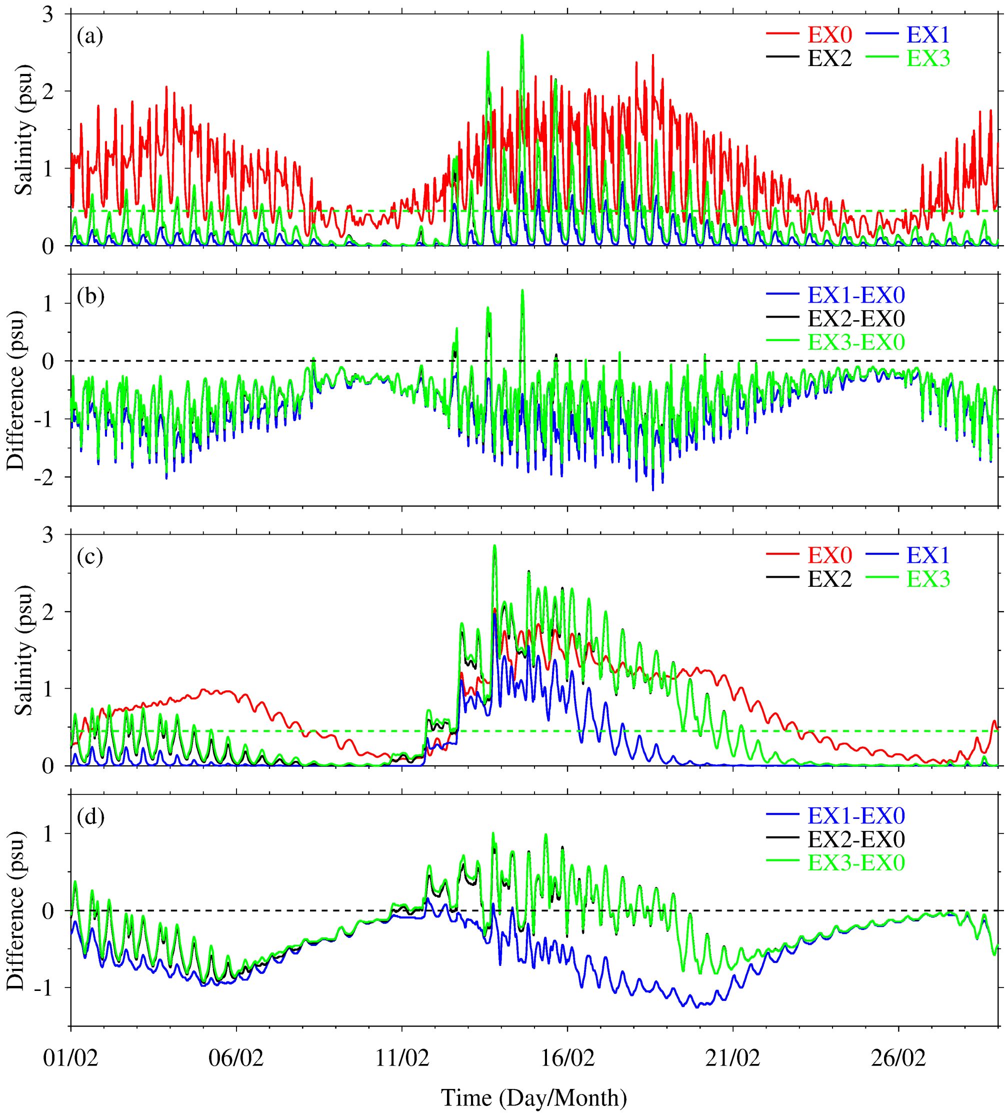

Figure 13. Modeled temporal variations in surface salinity (**a**,**c**) and difference in salinity (**b**,**d**) at the Dongfeng Xisha Reservoir (**a**,**b**) and Taicang Reservoir (**c**,**d**). In (**a**,**c**), green dashed line: 0.45 psu. In (**b**,**d**), black dashed line: 0 psu.

The Taicang Reservoir is located at the south coast of the middle reaches of the SB. In EX0, salinity below 0.45 psu was only observed during the neap tide, while saltwater intrusion occurred at other times (Figure 13c,d). The surface salinity and the duration of the available water intake time in February were 0.71 and 10.82 days, respectively. In EX1, the salinity exceeded the drinking water salinity standards around 13 February, which is attributed to saltwater intrusion from the NC. After the construction of sluice 1, except for the period of severe saltwater intrusion from the NC, the salinity decreased significantly during other times, with a maximum value of 1.2 psu. The surface salinity and the available water intake time in February were 0.19 and 23.56 days, respectively. Compared to EX0, the available water intake time increased by 12.74 days. In EX2, the saltwater intrusion from the NC intensified, and the salinity significantly exceeded the salinity standards in mid-February. After the construction of sluice 2, except for the period of severe saltwater intrusion from the NC, the salinity decreased substantially at most times, with a maximum value of 1.0 psu. The surface salinity and the available water intake time in February were 0.49 and 18.24 days, respectively. Compared to EX0, the available water intake time increased by 7.42 days. In EX3, the salinity variations were similar to those in EX2. The surface salinity and the available water intake time in February were 0.52 and 17.65 days, respectively. Compared to EX0, the available water intake time increased by 6.83 days.

The Chenhang Reservoir is located at the south side of the middle reaches of the SB, downstream of the Taicang Reservoir. In EX0, the saltwater intrusion after 13 February was primarily caused by saltwater intrusion from the NC (Figure 14a,b). The maximum surface salinity was approximately 2.8 psu. The surface salinity and the available water intake time in February were 0.85 and 9.31 days, respectively. In EX1, except for the period of saltwater intrusion from the NC, the salinity decreased significantly at other times, with a maximum value of 1.2 psu. The surface salinity and the available water intake time in February were 0.40 and 19.69 days, respectively. Compared to EX0, the available water intake time increased by 10.38 days. In EX2, there was no saltwater spillover from the NB, but the saltwater intrusion was enhanced downstream from the NC. The salinity was higher during the flood tide, and freshwater appeared during the ebb tide. There were periods of salinity decrease during the neap tide. The surface salinity and the available water intake time in February were 0.91 and 12.79 days, respectively. Compared to EX0, the available water intake time increased by 3.48 days. In EX3, the salinity variations were similar to those in EX2. The surface salinity and the available water intake time in February were 0.94 and 12.49 days, respectively. Compared to EX0, the available water intake time increased by 3.18 days.

The QCSR is located at the upper reaches of the NC. In EX0, only intermittent periods of freshwater appeared after the 25 February, with a maximum value of approximately 11 psu (Figure 14c,d). The surface salinity and the available water intake time in February were 2.28 and 1.02 days, respectively. In EX1, the salinity at the water intake of the QCSR decreased most of the time. With the disappearance of saltwater spillover from the NB, the salinity decreased during the middle tide after the spring tide. The surface salinity and the available water intake time in February were 2.10 and 4.22 days, respectively. Compared to EX0, the available water intake time increased by 3.2 days. In EX2, the salinity at the water intake of the QCSR increased significantly. The surface salinity and the available water intake time in February were 3.48 and 0.08 days, respectively. Compared to EX0, the available water intake time decreased by 0.94 days. In EX3, the salinity increase became even more pronounced. The surface salinity and the available water intake time in February were 3.55 and 0.05 days, respectively. Compared to EX0, the available water intake time decreased by 0.97 days. This further disadvantaged the water intake of the QCSR.

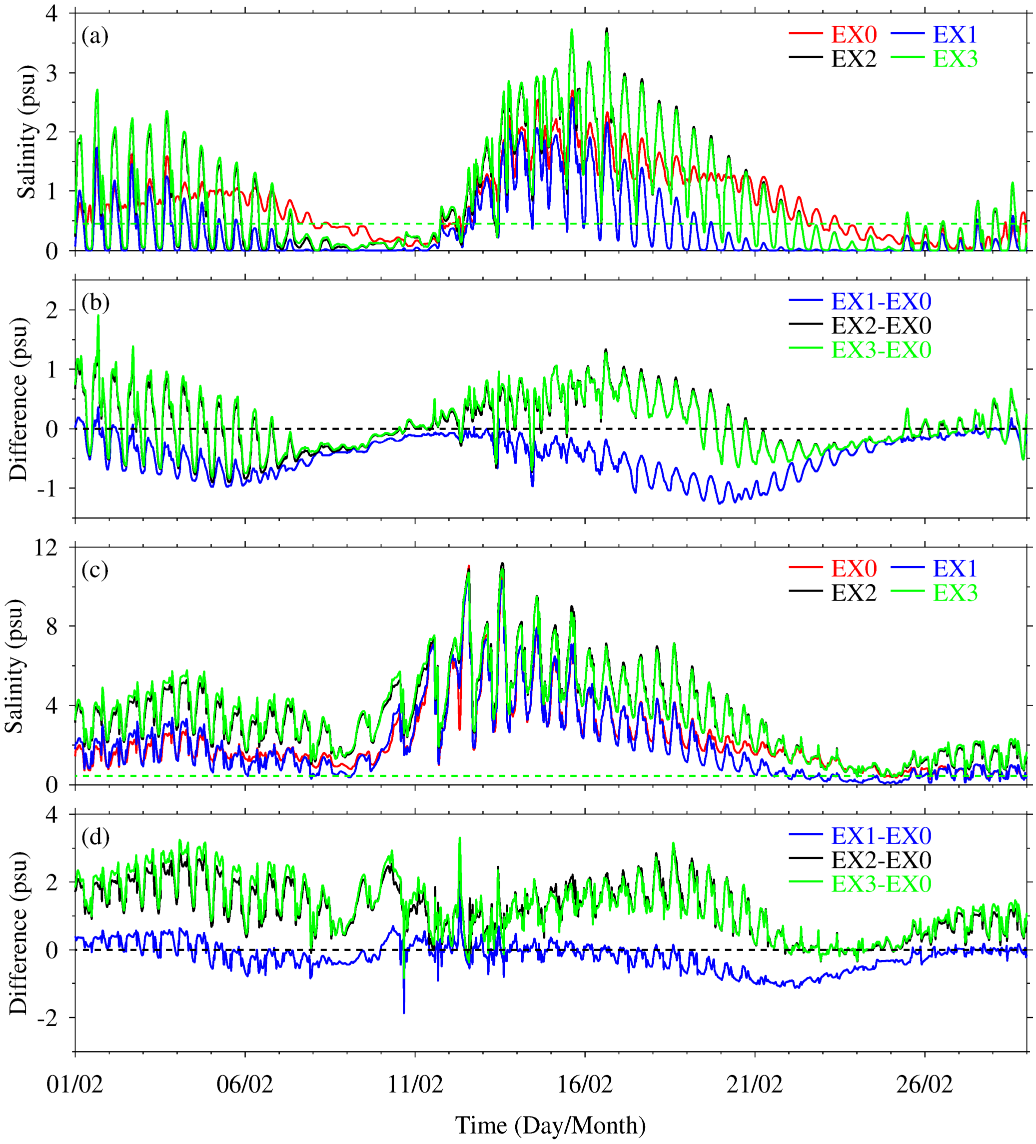

Figure 14. Modeled temporal variations in surface salinity (**a**,**c**) and difference in salinity (**b**,**d**) at the Chenhang Reservoir (**a**,**b**) and QCSR (**c**,**d**). In (**a**,**c**), green dashed line: 0.45 psu. In (**b**,**d**), black dashed line: 0 psu.

4. Discussion

The impacts of the sluices at different reaches of the NB on the saltwater intrusion and freshwater are analyzed in the previous sections. In this section, we discuss the different impacts on the salinity among the three sluices.

Compared to EX1, the NTWF across S1 in EX2 increased by 1493 m^3/s and 3202 m^3/s during the neap tide and spring tide (Table 2), respectively, resulting in the salinity in the entire NB and east of Chongming Island being much lower in EX2 than in EX1, with maximum values of less than 5.0 psu during the neap tide and 10.0 psu during the spring tide (Figure 15a,b). During the neap tide, the salinity decrease in EX2 was much greater than that in EX1 in the areas east of Chongming Island, the middle and lower reaches of the NC, and the lower reaches of the North Passage. The NTWF across S2 decreased by 1402 m^3/s and 3013 m^3/s during the neap tide and spring tide, respectively, resulting in more severe saltwater intrusion from the NC downstream and salinity increases in the SB, SC, upper reaches of the NC, North Passage, and South Passage. In the lower reaches of the NC, the salinity decreased during the neap tide and increased during the spring tide due to the effect of strong northerly winds, and the northward tidal Stoke and pumping water transport were weak during the neap tide.

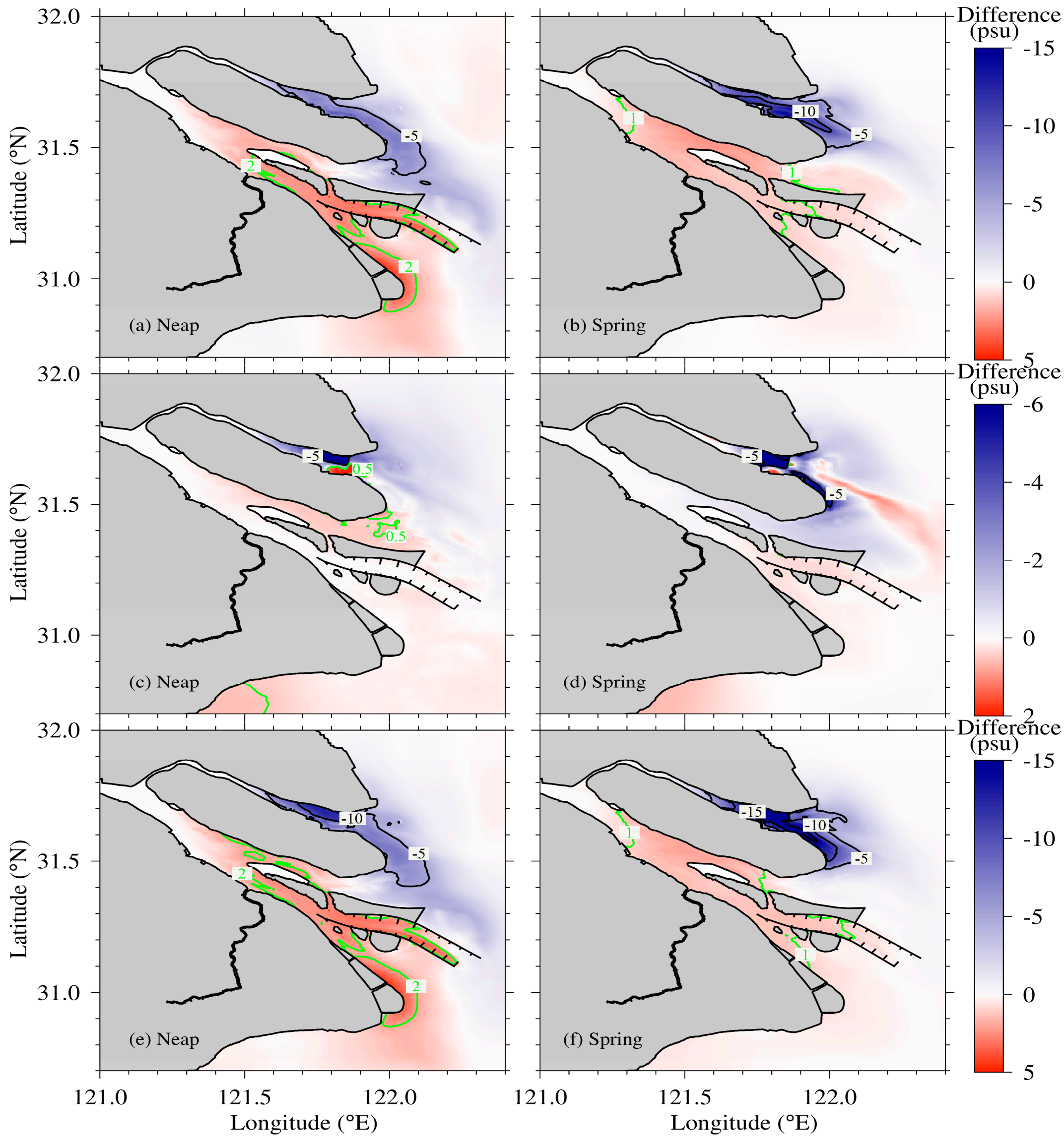

Figure 15. Differences in the tidally and vertically averaged salinity during neap tide (**left**) and spring tide (**right**) between EX2 and EX1 (**a**,**b**), EX3 and EX2 (**c**,**d**), and EX3 and EX1 (**e**,**f**).

Compared to EX2, the NTWF across S1 in EX3 changed by -501 m^3/s and 104 m^3/s during the neap tide and spring tide, respectively, due to weaker tidal dynamics during the neap tide, strengthening the salinity front (Figure 15c). The landward baroclinic force weakened the seaward water transport. Therefore, the decrease in salinity downstream of sluice 3 was much smaller during the neap tide than during the spring tide. The NTWF across S2 changed by -506 m^3/s and 78 m^3/s during the neap tide and spring tide, respectively, resulting in slight increases in salinity in the SB, SC, North Passage, and South Passage, especially in the NC, during the neap tide, and decreases in the SB, SC, and South Passage, especially in the NC, during the spring tide.

Compared to EX1, the NTWF across S1 in EX3 increased by 992 m^3/s and 3306 m^3/s and that across S2 decreased by 1031 m^3/s and 2935 m^3/s during the neap tide and spring tide, respectively. This NTWF change led to the salinity in the entire NB and east of Chongming Island being much lower in EX3 than in EX1, and the salinity in the SB, SC, upper reaches of the NC, North Passage, and South Passage was much higher in EX3 than in EX1 (Figure 15e,f). The pattern of the salinity change, and the cause of it, are more similar to the case of EX2 compared to that of EX1.

For the water intake at the water resources in the SB, sluice 1 in EX1 was distinctly better than sluice 2 in EX2 and sluice 3 in EX3, and sluice 2 was slightly better than sluice 3.

5. Conclusions

The outstanding feature of the saltwater intrusion is the saltwater spillover from the NB into the SB, which threatens the water intake of water resources in the SB. The construction of sluices in the NB can cut off the saltwater spillover from the NB and improve the safety of the freshwater supply for Shanghai. This study used the improved ECOM to simulate and assess the impacts of sluice construction in the upper, middle, and lower reaches of the NB on the saltwater intrusion and freshwater. The severe saltwater intrusion event in February 2014 was considered in a simulated scenario.

The simulation results show that, on the one hand, sluice construction in the upper, middle, and lower reaches of the NB can eliminate saltwater spillover from the NB into the SB, which is conducive to the intake of water resources in the SB; on the other hand, sluice construction increases the amount of water entering the NB from the SB during both the spring and neap tides, and the runoff discharging into the sea in the SB obviously decreases, resulting in saltwater intrusion increases in the NC and SC, which is not conducive to the intake of water resources in the SB.

Sluice construction in the upper, middle, and lower reaches of the NB increases the available water intake time by 18.77, 15.62, and 15.33 days for the Dongfeng Xisha Reservoir, by 12.74, 7.42, and 6.83 days for the Taicang Reservoir, and by 10.38, 3.48, and 3.18 days for the Chenhang Reservoir, respectively. For the QCSR, sluice construction in the upper reaches of the NB increases the available water intake time by 3.2 days, while sluice construction in the middle and lower reaches of the NB decreases the available water intake time by 0.97 and 0.94 days, respectively. The comprehensive effect of sluice construction in the NB is conducive to the water intake of the Dongfeng Xisha, Taicang, and Chenhang reservoirs, but only the sluice in the upper reaches of the NB is conducive to the water intake of the QCSR, while the sluices in the middle and lower reaches are not conducive to the water intake of the QCSR.

From the perspective of the impact of sluice construction in the NB on the saltwater intrusion and freshwater resources, it is recommended that a sluice be built in the upper reaches of the NB, which would be beneficial for the water intake in the QCSR, which supplies 50% of the freshwater for Shanghai.

Author Contributions: Conceptualization, Y.Y. and J.Z.; data curation, Y.Y. and R.M.; formal analysis, Y.Y. and Z.C.; investigation, Y.Y. and Z.C.; methodology, Y.Y. and J.Z.; project administration, J.Z.; resources, Y.Y. and J.Z.; software, Y.Y., J.Z. and R.M.; supervision, J.Z.; validation, Y.Y. and R.M.; visualization, Y.Y. and R.M.; writing—original draft, Y.Y.; writing—review and editing, J.Z. All authors have read and agreed to the published version of the manuscript.

Funding: This work was supported by the National Natural Science Foundation of China (42276174) and the National Key R&D Program of China (2022YFA1004404).

Institutional Review Board Statement: Not applicable.

Informed Consent Statement: Not applicable.

Data Availability Statement: Sea-surface wind data obtained from the ECMWF are available at https://cds.climate.copernicus.eu (accessed on 10 July 2023). Tidal constituents were obtained from the TPXO dataset (https://www.tpxo.net/otps, accessed on 10 July 2023). All datasets used in this study will be uploaded onto https://figshare.com/ (accessed on 18 July 2023).

Acknowledgments: We acknowledge the anonymous reviewers for their valuable comments and suggestions.

Conflicts of Interest: The authors declare no conflict of interest. The funders had no role in the design of the study; in the collection, analyses, or interpretation of the data; in the writing of the manuscript; or in the decision to publish the results.

References

1. Bowden, K.F.; Sharaf El Din, S.H. Circulation, Salinity and River Discharge in the Mersey Estuary. *Geophys. J. Int.* **1966**, *10*, 383–399. [CrossRef]
2. Sassi, M.G.; Hoitink, A.J.F.; de Brye, B.; Vermeulen, B.; Deleersnijder, E. Tidal impact on the division of river discharge over distributary channels in the Mahakam Delta. *Ocean. Dynam* **2011**, *61*, 2211–2228. [CrossRef]
3. Simpson, J.H.; Brown, J.; Matthews, J.; Allen, G. Tidal Straining, Density Currents, and Stirring in the Control of Estuarine Stratification. *Estuaries* **1990**, *13*, 125–132. [CrossRef]
4. Gong, W.; Shen, J. The response of salt intrusion to changes in river discharge and tidal mixing during the dry season in the Modaomen Estuary, China. *Cont. Shelf Res.* **2011**, *31*, 769–788. [CrossRef]
5. Zhu, J.; Cheng, X.; Li, L.; Wu, H.; Gu, J.; Lyu, H. Dynamic mechanism of an extremely severe saltwater intrusion in the Changjiang estuary in February 2014. *Hydrol. Earth Syst. Sc.* **2020**, *24*, 5043–5056. [CrossRef]
6. Valle-Levinson, A.; Wong, K.; Bosley, K.T. Response of the lower Chesapeake Bay to forcing from Hurricane Floyd. *Cont. Shelf Res.* **2002**, *22*, 1715–1729. [CrossRef]
7. Li, M.; Zhong, L.; Boicourt, W.C.; Zhang, S.; Zhang, D.-L. Hurricane-induced storm surges, currents and destratification in a semi-enclosed bay. *Geophys. Res. Lett.* **2006**, *33*, L2604. [CrossRef]
8. Li, C.; Weeks, E.; Rego, J.L. In situ measurements of saltwater flux through tidal passes of Lake Pontchartrain estuary by Hurricanes Gustav and Ike in September 2008. *Geophys. Res. Lett.* **2009**, *36*, L19609. [CrossRef]
9. Gong, W.; Lin, Z.; Chen, Y.; Chen, Z.; Zhang, H. Effect of winds and waves on salt intrusion in the Pearl River estuary. *Ocean. Sci.* **2018**, *14*, 139–159. [CrossRef]
10. Costa, Y.; Martins, I.; de Carvalho, G.C.; Barros, F. Trends of sea-level rise effects on estuaries and estimates of future saline intrusion. *Ocean. Coast. Manag.* **2023**, *236*, 106490. [CrossRef]
11. Guerra-Chanis, G.E.; Laurel-Castillo, J.A.; Schettini, C.A.; Kakoulaki, G.; Souza, A.J.; Valle-Levinson, A. Saltwater intrusion in estuaries with different dynamic depths. *Reg. Stud. Mar. Sci.* **2022**, *51*, 102186. [CrossRef]
12. Hong, B.; Shen, J. Responses of estuarine salinity and transport processes to potential future sea-level rise in the Chesapeake Bay. *Estuar. Coast. Shelf Sci.* **2012**, *104–105*, 33–45. [CrossRef]
13. Bhuiyan, M.J.A.N.; Dutta, D. Assessing impacts of sea level rise on river salinity in the Gorai river network, Bangladesh. *Estuar. Coast. Shelf Sci.* **2012**, *96*, 219–227. [CrossRef]
14. Wu, S.; Cheng, H.; Xu, Y.; Li, J.; Zheng, S. Decadal changes in bathymetry of the Yangtze River Estuary: Human impacts and potential saltwater intrusion. *Estuar. Coast. Shelf Sci.* **2016**, *182*, 158–169. [CrossRef]
15. Webber, M.; Li, M.T.; Chen, J.; Finlayson, B.; Chen, D.; Chen, Z.Y.; Wang, M.; Barnett, J. Impact of the Three Gorges Dam, the South–North Water Transfer Project and water abstractions on the duration and intensity of salt intrusions in the Yangtze River estuary. *Hydrol. Earth Syst. Sc.* **2015**, *19*, 4411–4425. [CrossRef]
16. An, Q.; Wu, Y.; Taylor, S.; Zhao, B. Influence of the Three Gorges Project on saltwater intrusion in the Yangtze River Estuary. *Environ. Geol.* **2009**, *56*, 1679–1686. [CrossRef]
17. Han, Z.; Pan, C.; Yu, J.; Chen, H. Effect of large-scale reservoir and river regulation/reclamation on saltwater intrusion in Qiantang Estuary. *Sci. China Ser. B* **2001**, *44*, 221–229, (In Chinese with English Abstract). [CrossRef]
18. Huan-ting, S.; Zhichang, M.; YuLiang, G. Impact of South-North water transfer (east route) on saltwater intrusion in the Changjiang estuary with consideration of its countermeasures. *Resour. Environ. Yangtze Basin* **2002**, *11*, 150–154, (In Chinese with English Abstract).
19. Andrews, S.W.; Gross, E.S.; Hutton, P.H. Modeling salt intrusion in the San Francisco Estuary prior to anthropogenic influence. *Cont. Shelf Res.* **2017**, *146*, 58–81. [CrossRef]
20. Kolb, P.; Zorndt, A.; Burchard, H.; Gräwe, U.; Kösters, F. Modelling the impact of anthropogenic measures on saltwater intrusion in the Weser estuary. *Ocean. Sci.* **2022**, *18*, 1725–1739. [CrossRef]
21. Ralston, D.K.; Geyer, W.R. Response to Channel Deepening of the Salinity Intrusion, Estuarine Circulation, and Stratification in an Urbanized Estuary. *J. Geophys. Res. Ocean.* **2019**, *124*, 4784–4802. [CrossRef]
22. Fox, J.P.; Mongan, T.R.; Miller, W.J. Trends in freshwater inflow to San Francisco Bay from the Sacramento–San Joaquin Delta. *J. Am. Water Resour.* **1990**, *26*, 101–116. [CrossRef]
23. Deng, Y.; Young, C.; Fu, X.; Song, J.; Peng, Z.-R. The integrated impacts of human activities and rising sea level on the saltwater intrusion in the east coast of the Yucatan Peninsula, Mexico. *Nat. Hazards* **2017**, *85*, 1063–1088. [CrossRef]
24. Xue, P.; Chen, C.; Ding, P.; Beardsley, R.C.; Lin, H.; Ge, J.; Kong, Y. Saltwater intrusion into the Changjiang River: A model-guided mechanism study. *J. Geophys. Res.* **2009**, *114*, C02006. [CrossRef]
25. Mao, Z.; Shen, H.; Liu, T.J.; Eisma, D. Types of saltwater intrusion of the Changjiang Estuary. *Sci. China. Ser. B Chem.* **2001**, *44*, 150–157. [CrossRef]
26. Tang, J.H.; Xu, J.Y.; Zhao, S.W.; Liu, W.Y. Research on saltwater intrusion of the south branch of the Changjiang estuary based on measured data. *Resour. Environ. Yangtze Basin* **2011**, *20*, 677–684, (In Chinese with English Abstract).

27. Obodoefuna, D.C.; Fan, D.; Guo, X.; Li, B. Highly accelerated siltation of abandoned distributary channel in the Yangtze Delta under everchanging social-ecological dynamics. *Mar. Geol.* **2020**, *429*, 106331. [CrossRef]
28. Werner, A.D.; Bakker, M.; Post, V.E.; Vandenbohede, A.; Lu, C.; Ataie-Ashtiani, B.; Simmons, C.T.; Barry, D. Seawater intrusion processes, investigation and management: Recent advances and future challenges. *Adv. Water Resour.* **2013**, *51*, 3–26. [CrossRef]
29. Post, V.E.A. Fresh and saline groundwater interaction in coastal aquifers: Is our technology ready for the problems ahead? *Hydrogeol. J.* **2005**, *13*, 120–123. [CrossRef]
30. Moore, W.S.; Joye, S.B. Saltwater Intrusion and Submarine Groundwater Discharge: Acceleration of Biogeochemical Reactions in Changing Coastal Aquifers. *Front. Earth Sci.* **2021**, *9*, 600710. [CrossRef]
31. Xu, Z.; Ma, J.; Wang, H.; Hu, Y.; Yang, G.; Deng, W. River Discharge and Saltwater Intrusion Level Study of Yangtze River Estuary, China. *Water-Sui* **2018**, *10*, 683. [CrossRef]
32. Gu, J.; Yang, J.Z.; Chen, W.; Qin, X.; Ma, D.Q.; Wang, X.L. Numerical Analysis of the Influence of Saltwater Intrusion on Qingcaosha Reservoir. *Appl. Mech. Mater.* **2012**, *212–213*, 216–220. [CrossRef]
33. Kwak, D.-H.; Song, Y.-S.; Choi, Y.-H.; Kim, K.-M.; Jeong, Y.-H. Influence of sluice gate operation on salinity stratification and hypoxia development in a brackish estuary dam. *Reg. Stud. Mar. Sci.* **2023**, *57*, 102731. [CrossRef]
34. Lan, X.; Zhang, H.; Wang, J.; Xu, J. Environmental impacts of building sluice on river estuary of Zhejiang Province. *Water Resour. Prot.* **2015**, *31*, 79–83, (In Chinese with English Abstract). [CrossRef]
35. Yang, X.; Wen, F.; Yaqun, Z. Benefits of building estuarine tidal gates in China and other countries and its impact analysis. *China Water Resour.* **2017**, *14*, 25–28, (In Chinese with English Abstract). [CrossRef]
36. Blumberg, A.F.; Mellor, G.L. *A Description of a Three-Dimensional Coastal Ocean Circulation Model*; Heaps, N.S., Ed.; American Geophysical Union: Washington, DC, USA, 1987; pp. 1–16. ISBN 0875902537/9780875902531.
37. Chen, C.; Zhu, J.; Zheng, L.; Ralph, E.; Budd, J.W. A Non-orthogonal Primitive Equation Coastal Ocean Circulation Model: Application to Lake Superior. *J. Great Lakes Res.* **2004**, *30*, 41–54. [CrossRef]
38. Wu, H.; Zhu, J. Advection scheme with 3rd high-order spatial interpolation at the middle temporal level and its application to saltwater intrusion in the Changjiang Estuary. *Ocean Model.* **2010**, *33*, 33–51. [CrossRef]
39. Egbert, G.D.; Erofeeva, S.Y. Efficient Inverse Modeling of Barotropic Ocean Tides. *J. Atmos. Ocean Tech.* **2002**, *19*, 183–204. [CrossRef]
40. Editorial Board for Marine Atlas. *Ocean Atlas in Huanhhai Sea and East China Sea (Hydrology)*; China Ocean Press: Beijing, China, 1992. (In Chinese)
41. Lü, H.; Zhu, J.; Chen, Q.; Li, M.; Pan, S.; Chen, S. Impact of estuarine reclamation projects on saltwater intrusion and freshwater resource. *J. Oceanol. Limnol.* **2022**, *41*, 38–56. [CrossRef]
42. Chen, Q.; Zhu, J.; Lyu, H.; Pan, S.; Chen, S. Impacts of topography change on saltwater intrusion over the past decade in the Changjiang Estuary. *Estuar. Coast. Shelf Sci.* **2019**, *231*, 106469. [CrossRef]
43. Nash, J.; Sutcliffe, J. River flow forecasting through conceptual models part I—A discussion of principles. *J. Hydrol.* **1970**, *10*, 282–290. [CrossRef]